Master in Chemical Engineering

Functionalized phosphorous carbon materials derived from biomass for supercapacitor application

A Master's dissertation

of

Miguel Ângelo Carneiro Granja

Developed within the course of dissertation

held in

Faculdade de Engenharia da Universidade do Porto

Supervisor at FEUP: **Dr. Natalia Rey Raap**

Co-Supervisor at FEUP: **Prof. Manuel Fernando Pereira**

U.PORTO
FEUP FACULDADE DE ENGENHARIA
UNIVERSIDADE DO PORTO

Departamento de Engenharia Química

July of 2018

“So that’s how it works. You plod along, putting one foot before the other, look up, and suddenly, there you are**.** Right where you wanted to be all along."

The Elder Scrolls IV: Oblivion

Acknowledgments

Este trabalho foi financiado por: Projeto POCI-01-0145-FEDER-006984 - Laboratório Associado LSRE-LCM - financiado pelo Fundo Europeu de Desenvolvimento Regional (FEDER), através do COMPETE2020 – Programa Operacional Competitividade e Internacionalização (POCI) e por fundos nacionais através da Fundação para a Ciência e a Tecnologia I.P.

Queria começar por agradecer à minha orientadora de tese, Dra. Natalia Rey Raap, por toda a sua orientação, disponibilidade e sobretudo pelo incentivo e simpatia dada ao longo destes 5 meses. O meu mais sincero obrigado.

Gostaria de agradecer também ao meu co-orientador, Professor Manuel Fenando Pereira, por toda a disponibilidade e apoio dado durante a realização do trabalho.

Queria agradecer a todas as pessoas do LCM, que durante este estágio curricular, deram-me as melhores condições possíveis.

Não podia deixar de agradecer ao meu amigo Rafael Morais, o destino fez-nos amigos no décimo ano e desde então nunca nos separou, até mesmo no estágio!

A vida não era a mesma sem eles, queria agradecer a todos os meus amigos, ao BdC e aos Brous, vocês fizeram esta experiência valer a pena.

À minha família, em especial à minha avó Clarinha pela bondade que sempre demonstrou para comigo e que sempre me fez acreditar que tudo é possível.

E por último, queria agradecer às pessoas mais importantes da minha vida, a minha mãe e o meu pai, que fizeram de mim a pessoa que sou hoje, devo-lhes tudo o que tenho. Obrigado por todo o amor.

Abstract

The development of new and greener technologies for energy conversion and storage has been highlighted in the last decades. Batteries are the most common energy storage devices, due to their high specific energy, however batteries present low specific power and low life-cycle. In contrast, supercapacitors (SCs) have higher specific power and great cyclability, which proves to be a promising technology for energy storage. Supercapacitors are constituted of two electrodes, a separator and an electrolyte solution. The electrodes are one of the main components of a supercapacitor due to their capability of enhancing the amount of energy stored. Carbon-based electrodes such as activated carbons, mesoporous carbons, carbon nanotubes or graphene have been widely investigated in supercapacitor applications due to their unique properties: high surface area, tailorable porosity and high electrical conductivity. Carbon materials can be prepared from a wide variety of precursors, although carbons prepared from renewable energy sources, like biomass-derived carbons, are presented as a promising solution for a sustainable future.

This work is focused in the preparation of phosphorus-functionalized biomass-derived carbons as electrode materials in supercapacitors. The work is divided into three distinctive parts: i) preparation of carbon materials by two distinctive methods: one-pot and impregnation; ii) evaluation of the electrochemical performance of the prepared materials in two and three-electrode cell configuration, and iii) determination of the relationship between the textural and chemical properties and the electrochemical performance of the materials. All materials were characterized by nitrogen adsorption-desorption isotherms at -196 ºC, scanning electron microscopy, elemental analysis, X-ray photoelectron spectroscopy, energy dispersive X-ray spectroscopy and temperature programmed desorption. The electrochemical performance was evaluated by cyclic voltammetry and galvanostatic charge-discharge methods.

This work allowed us to conclude that the textural and chemical surface properties of the studied materials depend on the preparation method and the carbonization temperature. Materials with different porosity and different degrees of functionalization were obtained. Impregnated sample treated at 800 ºC resulted in a surface area of 806 $m^2 g^{-1}$ and higher oxygen and phosphorous content (12.6 and 10.3 % respectively), being the formation and development of phosphorous containing groups strongly temperature-dependent. All prepared carbons were tested as electrode materials in supercapacitors. It was found that materials with higher surface areas and higher amount of phosphate groups give rise to higher capacitances (133 $F g^{-1}$).

Keywords (theme): biomass, carbon, phosphorous, supercapacitor, energy storage.

Resumo

Nas últimas décadas tem-se destacado o desenvolvimento de novas tecnologias mais ecológicas de conversão e armazenamento de energia. As baterias são os dispositivos de armazenamento de energia mais comuns, devido à sua alta energia específica, no entanto estas apresentam baixa potência específica e baixo ciclo de vida. Em contraste, os supercondesadores (SC) apresentam uma maior potência específica e grande ciclabilidade, o que prova ser uma tecnologia promissora para armazenamento de energia. Os supercondensadores são constituídos por dois elétrodos, um separador e uma solução eletrolítica. Os elétrodos são um dos principais componentes de um supercondensador devido à sua capacidade de aumentar a quantidade de energia armazenada. Os elétrodos de materiais à base de carbono, como carvão ativado, nanotubos de carbono ou grafeno, têm sido amplamente investigados em aplicações de supercondensadores devido às suas propriedades únicas: alta área superficial, porosidade adaptável e alta condutividade elétrica. Os materiais de carbono podem ser preparados a partir de uma ampla variedade de precursores, embora os materiais preparados a partir de fontes renováveis, como os carvões derivados da biomassa, sejam apresentados como uma solução promissora para um futuro sustentável.

Este trabalho foca-se na preparação de materiais de carbono derivados de biomassa funcionalizados com fósforo como materiais de elétrodo em supercondensadores. O trabalho dividiu-se em três partes distintas: i) preparação de materiais de carbono por dois métodos diferentes: "one-pot" e impregnação; ii) avaliação do desempenho eletroquímico dos materiais preparados em células de dois e três elétrodos; e iii) determinação da relação entre as propriedades texturais e químicas e o desempenho eletroquímico dos materiais. Todos os materiais foram caracterizados a partir de isotérmicas de adsorção-dessorção de nitrogénio a -196 ºC, microscopia eletrónica de varrimento, análise elementar, espectroscopia de fotoelétrões de raios X, espectroscopia de energia dispersiva de raios X e dessorção a temperatura programada. O desempenho eletroquímico efetuou-se por métodos de voltametria cíclica e carga-descarga galvanostática.

Este trabalho permitiu concluir que as propriedades texturais e químicas da superfície dos materiais estudados dependem do método de preparação e da temperatura de carbonização. Obtiveram-se materiais com diferentes porosidades e diferentes graus de funcionalização. A amostra impregnada a 800 ºC obteve-se uma área de superfície de 806 $m^2 g^{-1}$ e maior conteúdo de oxigénio e fósforo (12.6 e 10.3 % respectivamente). A formação e o desenvolvimento de grupos contendo fósforo dependem fortemente da temperatura. Testaram-se todos os materiais de carbono preparados como materiais de elétrodo em supercondensadores. Descobriu-se ainda que materiais com maiores áreas de superfície e maior quantidade de grupos fosfato dão origem a maiores capacidades (133 F g^{-1}).

Palavras chave: biomassa, carbono, fósforo, supercondensador, armazenamento de energia.

Declaration

I hereby declare, on my word of honour, that this work is original and that all non-original contributions were properly referenced with source identification.

Sign and date

Index

List of Figures

List of Tables

Notation and Glossary

A	Area	m^2
m	Active mass	g
I	Current Intensity	A
V_{meso}	Mesopore volume	$cm^3\ g^{-1}$
V_{DR}	Micropore volume	$cm^3\ g^{-1}$
M	Molar concentration	$mol\ dm^{-3}$
r	Scan rate	$V\ s^{-1}$
C_s	Specific capacitance	$F\ g^{-1}$
S_{BET}	Specific surface area	$m^2\ g^{-1}$
V	Voltage	V
dV	Voltage variation	V
Vw	Voltage window	V

Greek Letters

Δ	Variation

Indexes

*	dimensionless variable
i	index or counter
®	registered trademark symbol

List of Acronyms

BET	Brunauer-Emmet-Teller
CNT	Carbon nanotubes
DR	Dubbinin-Radushkevich
EDLC	Electric double layer capacitors
EDS	Energy dispersive X-ray spectroscopy
HTC	Hydrothermal carbonization
LSRE	Laboratory of Separation and Reaction Engineering
LCM	Laboratory of Catalysis and Materials
OHP	Outer Helmmoltz plane
SC	Supercapacitor
SEM	Scanning electron microscopy
TCD	Thermal conductivity detector
TPD	Temperature programmed desorption
XPS	X-ray photoelectron spectroscopy

1 Introduction

1.1 Framing and presentation of the work

The present work was developed in the Associate Laboratory LSRE-LCM, which is a partnership between LSRE – Laboratory of Separation and Reaction Engineering and LCM – Laboratory of Catalysis and Materials.

The rapidly population growth tide with the increasing demand of energy have been one of the main concerns for the sustainability of our planet. Many technologies are being improved for the storage and conversion of energy. Supercapacitors are a promising technology for storage energy, however present low specific energy. Therefore, to enhance their performance, it is necessary to develop new electrode materials. Carbon based electrodes are very promising materials as their properties can be tailored to fit the requirement of supercapacitors. The appropriate combination of those properties can provide supercapacitors with high capacitance. In addition, the use of biomass to produce carbon electrodes is consistent with a sustainable future.

The objective of this work consists in the study of the effect of phosphorous functionalities in biomass-derived carbon electrodes on the performance of supercapacitors. The work is divided into three distinctive parts: i) preparation of functionalized carbon materials derived from biomass with tailored porosity, ii) evaluation of the electrochemical performance of the prepared materials, iii) determination of the relationship between the textural and chemical properties and the electrochemical performance of the prepared carbons.

1.2 Contributions of the work

There are different strategies to enhance the capacitance of a supercapacitor: improving the surface area, improving the electrical conductivity and modifying the surface chemistry of the materials. To the present day, the synthesis of functionalized carbons with heteroatoms, such as oxygen and nitrogen, is one of most used techniques for improving the performance in supercapacitors. The study of the effects of other heteroatoms such as phosphorous and boron in supercapacitors is less known. The present work provides insight of two different synthesis methods for preparing phosphorus doped carbons. This work demonstrates that the preparation method impacts the prosphorous functionalization content and contributes to shed some light on how the different type of phosphorous groups affect the capacitance in supercapacitors.

1.3 Organization of the thesis

The present dissertation is organized in six chapters. The first chapter, in which these words are included, introduces the motivation of the work and explains some basic concepts. The framework within the research field is also explored, as well as the need to improve the actual technology of supercapacitors.

Chapter 2, Context and State of Art, presents the current energy demand problem and describes and compares the different energy storage systems. The most relevant features of the energy storage system studied in the present dissertation, supercapacitors, are emphasized. Moreover, the most important properties of carbon materials, to be used as electrodes for supercapacitors, are highlighted. Finally, a detailed description on the use of biomass-derived carbons as electrode materials in supercapacitors and the strategies that can be adopted to tailor their properties and enhance their electrochemical performance is described.

Chapter 3, Materials and Methods, describes the procedures used in the preparation of the studied materials and the equipment used in the characterization. The procedures and equipment used for evaluation of their performance as electrode materials are also described.

Chapter 4, Results and Discussion, presents the results obtained for all the characterization techniques, as well as a deep discussion and analysis of the most relevant outcomes.

Chapter 5, Conclusions, presents the main conclusions, framing the obtained results with the objectives of the work.

Lastly, chapter 6, Assessment of the Work Done, presents an evaluation of the work, mentioning all the limitation encountered and proposing ideas for future assignments.

2 Context and state of the art

The ever-growing consumption of energy as well as the need to substitute fossil-fuels due to their limited availability and increasing problems with the gas emissions and pollution have propelled the investment on new greener alternatives for converting and storing energy. Searching for renewable energy sources such as wind, solar, geothermal, hydropower or biomass is very important and could be the only sustainable solution for the future [1, 2].

Some of these renewable energy sources are intermittent, meaning that there is an urge for grid storing and distribution of large amounts of energy within seconds or minutes. Thereof, the development of energy storage systems providing an efficient supply in peaks of energy demand is the key to displace a petroleum-based economy.

In an energy storage device, there are two important features: the amount of electric energy stored, and the maximum power supplied. Figure 1 illustrates the Ragone plot, which compares specific power and specific energy of various energy storage devices.

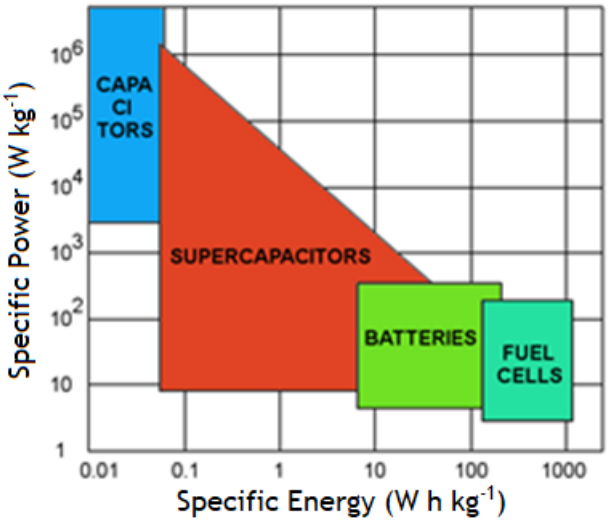

Figure 1- Ragone plot of various electrical energy storage system.

Batteries are the most common energy storage devices, which are widely used in light-duty vehicles as well as in smartphones, due to their high specific energy. However, supercapacitors, SCs, have been gaining more attention in the last decades due to their higher specific power, which is a feature of great importance in vehicles and for grid energy. Another main difference between batteries and supercapacitors is that, batteries store electrical energy indirectly, only

through redox reactions, while supercapacitors store energy via electrostatic and redox reactions. [3-5].

Table 1 shows a detail comparison between these two different storage systems.

Table 1 - Comparison between the properties of: supercapacitors and batteries

Characteristics	Supercapacitor	Battery
Specific energy (W h kg^{-1})	1 - 10	10-100
Specific power (W kg^{-1})	500 – 10,000	< 1000
Discharge time	s to min	0.3-3 h
Charge time	S to min	1-5 h
Cycle-life	>500,000	About 1000

One of the main problems of supercapacitors is their low specific energy compared to batteries. Besides, they have poor volume energy density and require stacking for high potential operations, which translates in excessive costs of fabrication [3]. Despite these drawbacks, supercapacitors exhibit some interesting features such as long-life cycle, high reversible charge-storage process [6], simple construction and ability to complement with other energy storage devices for hybrid applications. The most important advantages and disadvantages of supercapacitors are shown in Table 2.

Table 2 – Summary of supercapacitors characteristics

Advantages	Disadvantages
High power density	Limited specific energy
High reversible charge-storage process	Poor volume density
Very versatile (can be used in hybrid application)	Require stacking for high potential operation
Long life-cycle	

All these advantages make supercapacitors very promising devices suitable in a large number of applications [3, 5, 6]. Currently, three main sectors take advantage of SCs:

- Automotive industry: with the emergence of hybrid-electric vehicles, supercapacitors have gained more attention in this sector, especially, in stop-go hybrid vehicles, and electrical braking systems. In addition, merging supercapacitors with car batteries is also an interesting topic, peak loads outcoming from car's acceleration, can be overcome by the use of a supercapacitor [2, 7, 8].
- Energy supply: supercapacitors are a good alternative as energy storage device, as it can improve the reliability and quality of the grid energy distribution. For example, solar or wind energy can be stored in a SC during the day and be then available to be used during peak hours. They could also be implemented as portable power supplies, as they are suited to act as rechargeable stand-alone power sources[2, 8].
- Electronic industry: although it is difficult for supercapacitors to compete directly with batteries due to their lower energy density, the versatility of SCs can make them also useful in this area. In fact, SCs can be merged with batteries, to maximize the overall life cycle or can act merely as an energy storage system, making them an interesting option for cameras, mobile-phones or computers [7, 9].

Further breakthroughs to improve the performance of supercapacitors and develop more cost-effective components are essential to strengthen the usability of the SCs in daily lives technology. To this end, it is necessary to know the most important ins and outs of the components of a supercapacitor and fully understand the internal mechanisms.

2.1 Supercapacitors

2.1.1 Main components of a supercapacitor

Supercapacitors consist of two electrodes separated by an ion-permeable separator and an electrolyte connecting both electrodes. A typical scheme of a supercapacitor cell is shown in Figure 2.

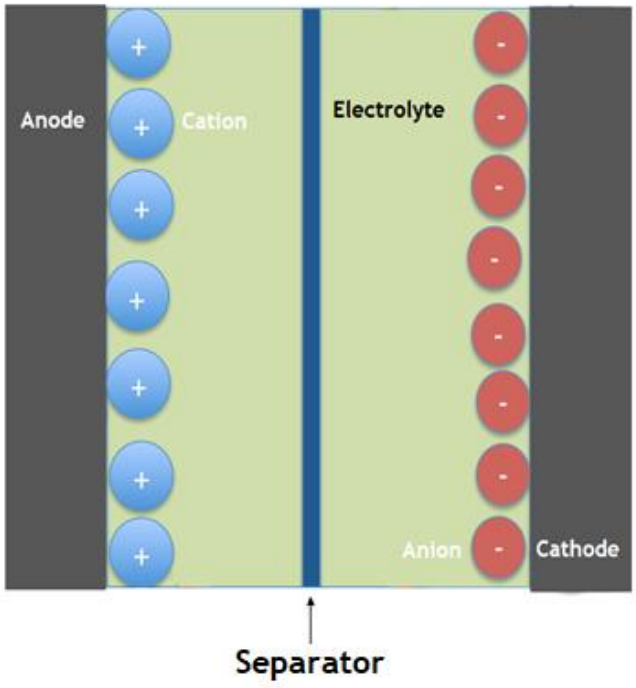

Figure 2 – Scheme of a standard supercapacitor.

The electrode is one of the main components of the SCs. Metal oxides, carbon-based materials and conductive polymers have been extensively studied as electrode materials for SCs. In fact, one of the best strategies to improve the capacitance, i.e. the specific power and energy, is to improve and develop new electrode materials.

The separator, as the name implies, physically separates the two electrodes and is usually a polymer that has a high ionic conductance, low thickness and good electrical resistance. The separator is also soaked with the electrolyte allowing the transfer of ions.

The performance of a SC is also dependent of the electrolyte employed, as it limits the attainable cell voltage (Table 3). For example, aqueous electrolytes like potassium hydroxide and sulphuric acid, have a breakdown voltage of around 1.2 V due to the breakdown voltage of water. On the other hand, organic electrolytes, like acetonitrile or propylene carbonate, have

higher breakdown voltages (around 3 V). However, it should be highlighted that organic electrolytes have higher resistivity [2].

Table 3 - Properties of different electrolytes adapted from reference [10]

Electrolyte	Density (g cm^{-3})	Resistivity (Ohm cm)	Cell voltage (V)
Potassium hydroxide	1.29	1.9	1.0
Sulfuric acid	1.2	1.35	1.0
Acetonitrile	0.78	18	2.5 - 3.0
Propylene carbonate	1.2	52	2.5 - 3.0

The selection of the appropriate components used to assembly the cell (electrode material, separator and type of electrolyte) is essential, as they have a direct effect on the internal mechanism by which the energy is storage.

2.1.2 Energy storage mechanism

Supercapacitors are energy storage devices capable of supplying high power density, i.e. fast energy delivery, which can be classified based on the energy storage mechanism. There are two storage principles: i) electric double layer capacitance and ii) pseudocapacitance [2].

2.1.2.1 Electric double layer capacitance

Electric double layer capacitors are the most common supercapacitors. The electrical energy is storage by electrostatic processes (non-Faradaic processes), in which an accumulation of charges is achieved in the interfaces of the two electrodes. The electric double layer is formed on the electrodes surface by applying a charge to the system (Figure 3).

There are three main theories for this type of mechanism:

- The Helmholtz model states that the charge of the solid electronic conductor is neutralized by the opposite sign ions at a distance, called outer Helmmoltz plane, OHP, which is the distance between the centre of the ions and the surface. This is the simplest theory and does not properly explain what occurs [11].

- The Gouy-Chapman model or the diffuse model states that the ions in the solution tend to diffuse into the liquid phase until the counter potential, set up by their departure, restricts this tendency [2, 11, 12].
- The Stern modification of the diffuse double layer draws near the Gouy-Chapman model, and states that the ions have a finite size, limiting their proximity to the surface. It is assumed that there can be a specific surface-adsorbed ion, also known as Stern layer. In this layer the ions are more adsorbed by the electrode surface [8, 11, 13].

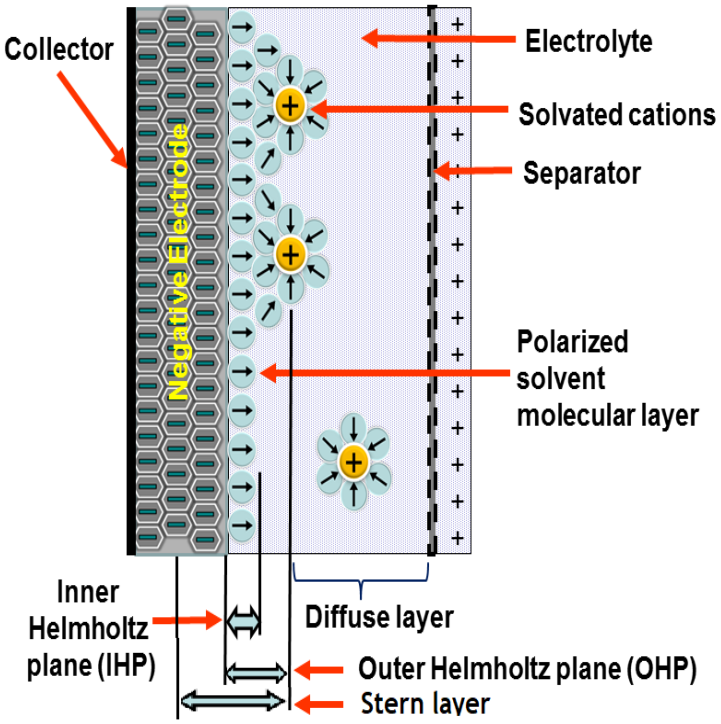

Figure 3 - Schematic representation of a EDLC.

When charging a supercapacitor, electrons move from the positive to the negative electrode through an external circuit. Anions concentrate in the positive electrode and cations in the negative electrode forming the electric double layer that compensates the external circuit. During the discharge, the reverse happens and both ions (cations and anions) became mixed in the porous structure [6, 13, 14].

The mobility of the ions depends on the pore size of the electrode materials as if the pores size is too small the ions cannot pass, affecting the capacitance of the supercapacitor [2].

2.1.2.2 **Pseudocapacitance**

Electrochemical pseudocapacitors store electrical energy by redox reactions (Faradaic-processes) between the electrolyte and the species on the surface of the electrode. Redox pseudocapacitance takes place when the ion is electrochemical adsorbed onto the electrode's surface, as shown in Figure 4 [14, 15].

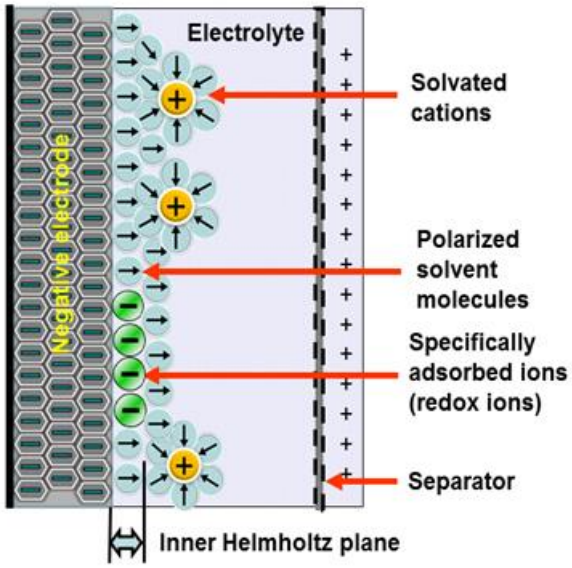

Figure 4 – Schematic representation of pseudocapacitors.

The pseudocapacitance can be 10-100 times higher than capacitance in an EDLC, due to the presence of Faradic reactions. However, electrodes that demonstrate pseudocapacitance behaviour, such as metal oxides or conducting polymers, are more incline to shrinking and swelling when charging or discharging, which can lower the life cycle and mechanical stability of a supercapacitor [14, 15].

2.1.3 Electrode material

Further improvements of the electrochemical performance of supercapacitors depend greatly on the development of new electrode materials. The type of mechanism, either its electrical double layer capacitance, pseudocapacitance or a combination of both, depends on the properties of the electrode materials. Consequently, further developments of new electrode materials are essential to improve the electrochemical performance of a supercapacitor. Many different materials have been studied as electrodes in supercapacitors, such as carbon materials, metal oxides or conducting polymers. Among all materials, carbon-based electrodes are the most promising for supercapacitors as they exhibit high surface area, excellent

electrical conductivity and controllable porosity. However, tailoring these properties is of great importance, specifically in terms of power and energy density. For example, materials with high surface area allows higher energy storage on the surface, while a good pore size distribution improves the charge transport. Accordingly, preparing new advanced carbon materials with tailored properties is an issue of major concern to improve the performance of supercapacitors.

2.2 Carbon materials

Carbon based materials such as activated carbons, carbon fibers, mesoporous carbons, carbon nanotubes or graphene oxide have been widely investigated in diverse fields of applications due to their unique properties, which involve high surface area, good electrical conductivity, high thermal conductivity and mechanical and chemical stability.

Carbon materials can be prepared from a wide variety of precursors and exist in various forms such as powders, fibers, nanotubes and nanospheres. Besides, some of their properties can be tailored to fit the requirements of the selected application.[2, 4, 16].

The most common strategies to tailor the properties of carbon materials are detailed below.

2.2.1 Textural properties

There are two main processes for obtaining carbon materials: i) carbonization and ii) activation.

Carbonization takes place at temperatures above 300 ºC for 2 to 4 h under an inert atmosphere. This process usually produces carbon materials with specific surface areas of around 600 $m^2 g^{-1}$ [17].

Activation process can be either a chemical or a physical process:

- Chemical activation is commonly performed at temperatures between 400-900 ºC. It involves the use of dehydrating agents such as phosphoric acid and zinc chloride or the use of oxidant agents like potassium hydroxide [18]. Potassium hydroxide is the most popular activation agent as it requires low activation temperature and gives rise to high carbon yields. This type of activation allows the control of pore size and produces carbon with high surfaces areas.

Figure 5 – Representation of a chemical activation.

- Physical activation is performed at temperatures between 400 and 1000 ºC in the presence of an oxidizing gas such as carbon dioxide or steam. This treatment allows the development of porosity resulting in materials with high surface area. In general, the carbon yield and pore wide decrease by increasing the temperature of activation, while the degree of activation increases.

When comparing chemical with physical activation, chemical activation needs lower process temperature, shorter activation time and results in higher carbon yield, while physical activation, results in materials with higher surface areas [19].

2.2.2 Chemical properties

The chemical properties of carbon materials can be altered by doping them with heteroatoms, such as oxygen [20], nitrogen [21], boron [22], sulphur [23] or phosphorus [24]. The precursors of such heteroatoms form functional groups that confers different characteristics to the surface. Introducing these functional groups can be achieved either "in-situ", during the preparation or synthesis process or "ex-situ", which involves thermal post-treatments [10]. The degree of functionalization and the nature of the incorporated functional groups depend on i) the precursor of the heteroatom employed, ii) the nature of the carbon material and iii) the temperature and time of the doping process.

Among all the heteroatoms mentioned above oxygen and nitrogen are the two most studied. For example, Sousa et al. [25], prepared nitrogen-doped carbon xerogels using nitrogen precursors (melamine or urea) via an "in-situ" doping method. It was observed that a variation on the temperature of carbonization (500, 700 and 900 ºC) originated carbon gels with different surface functionalities. On the other hand, Figueiredo et al. [26], studied different oxidation strategies in order to introduce oxygen functionalities via "ex-situ" method. The modification of oxidation conditions and performance of various thermal treatments after oxidation allowed

establishing correlations between the oxidation parameters and the type of functional groups introduced into the carbon material structure.

The introduction of heteroatoms increases the surface activity of carbon materials and modifies their electronic properties, which is of great importance in energy storage applications. These properties may be also altered by introducing metallic species such as Ni, Fe, Co or Mn, or by preparing hybrid materials. The development of the latter strategies has increased in recent years, as the combination of different allotropic forms of carbon allows to obtain hybrid materials with unique chemical properties. For example, both graphene and carbon nanotubes, CNTs, have been used to prepare hybrid carbon materials with improved electrical conductivity and thermal stability, which gives rise to high capacitances in supercapacitors [27, 28].

Graphene is a one-atom thick sheet made of sp^2 carbon bonds (Figure 6A). Graphene has great performances in energy storage devices, because of high rate and cycle capability, large surface area, high conductivity, good thermal and chemical stability and versatile [29]. The discovery of CNTs has deeply influenced the way carbon materials are designed due to their good electrical properties, good mechanical and thermal stability, and their unique structure [27, 28]. Their open tubular shape makes them good supports for active materials (Figure 6B); however, because of their hydrophobic property, the specific capacitance values are low (20 to 80 F g^{-1}) when compared to activated carbons [14, 30]. Despite being promising materials, both graphene and CNTs are costlier when compared with other carbons and carry environmental risk [31-33]. However, their ability to be coupled with other carbons, provides a good choice for supercapacitors applications.

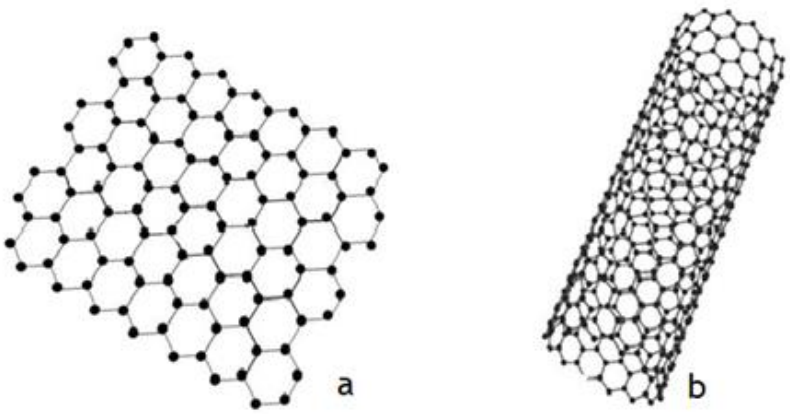

Figure 6 - Representation of two types of carbons: a- Graphene and b - Carbon nanotubes.

2.3 Biomass-derived carbons as electrode materials for supercapacitors

As explained above, carbon materials can be obtained by different precursors, i.e. such as petroleum coke-derived or graphite, which are limited and nonrenewable. However, carbons can also be attained by a greener sustainable alternative, such as biomass [34].

Biomass is an abundant and economic resource, composed of lignin, cellulose and hemicellulose. Biomass resources include energy crops, municipal wastes, animal wastes and aquatic plants and algae. The properties of biomass-derived carbons depend on the biomass precursors and the methods used to prepare the materials. There are different methods to transform biomass into carbon materials, such as high voltage electricity [4, 19], laser ablation or hydrothermal carbonization [35].

Among the different processes, hydrothermal carbonization (HTC) offers significant advantages, which involve low-energy process, high conversion efficiency and relatively moderate operating conditions. HTC is a low-cost procedure that takes place under low temperature (<230 ºC) in which pressure is self-generated. It facilitates hydrolysis and cleavage of the biomass constituents, giving rise to carbon structures [28, 36].

The valorization of biomass as a source of carbon materials through hydrothermal processes has emerged as an interesting alternative to produce electrode materials for supercapacitors. Although the carbons obtained by hydrothermal carbonization of biomass are environmental friendly, abundant and inexpensive, the energy density and power density provided still sets a drawback when comparing with other electrodes based on carbon materials, as well as poor mechanical resistance. Different strategies to improve the properties of biomass-derived carbons can be found in the literature. For example, the structural morphology can be modulated by modifying the synthesis conditions such as the concentration of the aqueous precursor solution, the temperature of the hydrothermal treatment, the reaction time and type of biomass precursor [37]. Besides, as previously mentioned, chemical or physical activation can be also applied to modify the textural properties [38]. The incorporation of different heteroatoms or advanced carbon materials into the initial precursor solution have been also reported as strategies to modify the textural and chemical properties.

Coupling with CNTs [28, 31], introducing heteroatoms such as phosphorous in the carbon surface [20, 22, 39], are some of the strategies adopted and studied in this dissertation. The work focus on the study of the effect of phosphorous in carbon electrodes, since there are not many studies using this heteroatom. There are two case studies, one in which the phosphoric acid acts as a precursor and the other as an activating agent.

3 Materials and methods

The main goal of this dissertation consists in the study of the effect of phosphorus functionalities on biomass-derived carbons used as electrode materials in supercapacitors.

Several carbons materials with different properties were prepared and characterized to determine the relationship between the phosphorous specification and the electrochemical performance.

The following subchapters describe all the procedures, materials and equipment used for the synthesis of the carbon materials, as well as for all the characterization tests.

3.1 Preparation of carbon materials

The carbon materials were prepared by hydrothermal carbonization using the following main reagents: D-glucose which represents the biomass, carbon nanotubes, distilled water and phosphoric acid (H_3PO_4).

The functionalization of the samples was performed by following two different methods i) by addition of phosphoric acid during the hydrothermal polymerization (from now on called one-pot method) and ii) by subsequent impregnation (from now on called impregnation method). After the incorporation of the phosphoric acid, the samples were treated in a vertical furnace at different temperatures in order to performed carbonization and chemical activation, respectively. Figure 7 shows a scheme of the methodology followed for the preparation of the different materials, which is explained below in more detail.

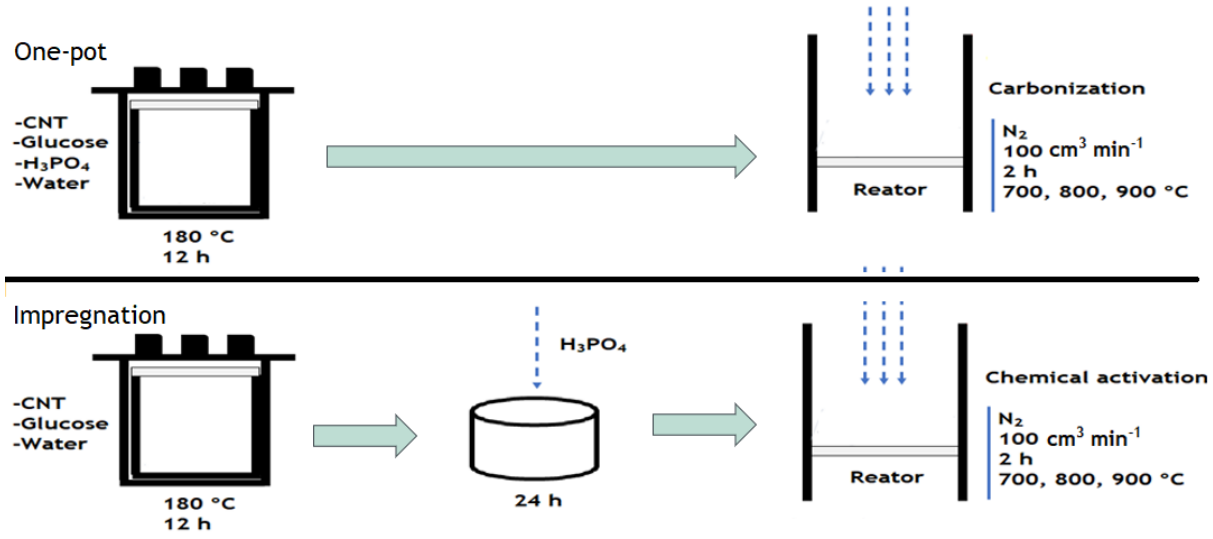

Figure 7 – A schematic representation of the methodology followed for the preparation of different carbon materials.

3.1.1 Hydrothermal treatment

Samples were prepared by dispersing 9 g of glucose and, 2 % (w/w) of carbon nanotubes (CNT) in 52 ml of distilled water in an unsealed glass baker under sonication for 30 min. The mixture was then introduced into a Teflon-lined in a stainless-steel autoclave and heated at 180 ºC for 12 h. After polymerization the resulting material was then recovered by filtration and washed with distilled water, until the attainment of a colorless aqueous phase. Finally, the material was dried at 80 ºC overnight. The resulting material is shown in Figure 8.

Figure 8 - Carbon prepared by hydrothermal treatment.

3.1.2 Doping methods

Phosphorous-doped carbons were prepared by following two different methods: one-pot method and impregnation method. The methods were conveyed differently to study the effect of introducing the phosphorous before and after the hydrothermal treatment.

3.1.2.1 One-pot method

In this method, phosphoric acid was added during the hydrothermal treatment. The samples were prepared by mixing 9 g of glucose with 2 % (w/w) of carbon nanotubes. The mixture was then dispersed in 52 ml of a 10:3 (w/w) distilled water/acid phosphoric solution under sonication for 30 min. Laterward the mixture was introduced into a Teflon-lined recipient and in a stainless-steel autoclave under hydrothermal treatment at 180 ºC, for 12 h was applied. The resulting material was then recovered by filtration and washed with distilled water until the attainment of a colorless aqueous phase. Lastly, the material was dried at 80 ºC overnight.

3.1.2.2 Impregnation method

The samples obtained by hydrothermal treatment (see details in section 3.1.1.), were impregnated with 9 ml of phosphoric acid and left in contact for one day to ensure an adequate impregnation of all the material. The impregnated sample was then washed with distilled water and dried at 80 ºC overnight. The aim of impregnating with phosphoric acid was: i) functionalize the surface with phosphorous functionalities and ii) use the acid as activating agent during the subsequent thermal treatment.

3.1.3 Thermal treatments

Thermal treatments were conveyed at different temperatures, to study the relationship between the temperature and the final properties of the carbon material.

Irrespective of the doping method, 2 g of each sample was weighed and then placed in a vertical furnace under nitrogen flow (100 cm^3 min^{-1}) and heated up at the selected temperature, which was maintained for 2 h. Three different temperatures were selected for the thermal treatments: 700, 800 and 900 ºC.

One-pot samples were denoted as CG_CNT_Pop_X, while carbons prepared by impregnation method were denoted as CG_CNT_P_X, where is X is the thermal temperature. For example, CG_CNT_Pop_700 was prepared by one pot method and carbonized at 700 ºC and CG_CNT_P_700 is a carbon prepared by the impregnation method and activated at 700 ºC.

For comparison purposes, a sample without phosphorous was prepared by hydrothermal treatment and subsequent carbonization at 700 ºC. This sample is denoted as CG_CNT.

In addition, two more samples were prepared by performing the thermal treatment under a different atmosphere to physically activate the samples. The methodology followed is shown in Figure 9. Two different samples were selected: i) one obtained directly from the hydrothermal treatment and ii) one prepared by the hydrothermal treatment followed by impregnation with phosphoric acid. The samples were physically activated with carbon dioxide with a flow of 160 cm^3 min^{-1}. Non-impregnated sample was physically activated at 850 ºC for 2 h, while impregnated sample was activated at 800 ºC for 4 h. These samples were labelled as AG_CNT_850 and AG_CNT_P_800 respectively.

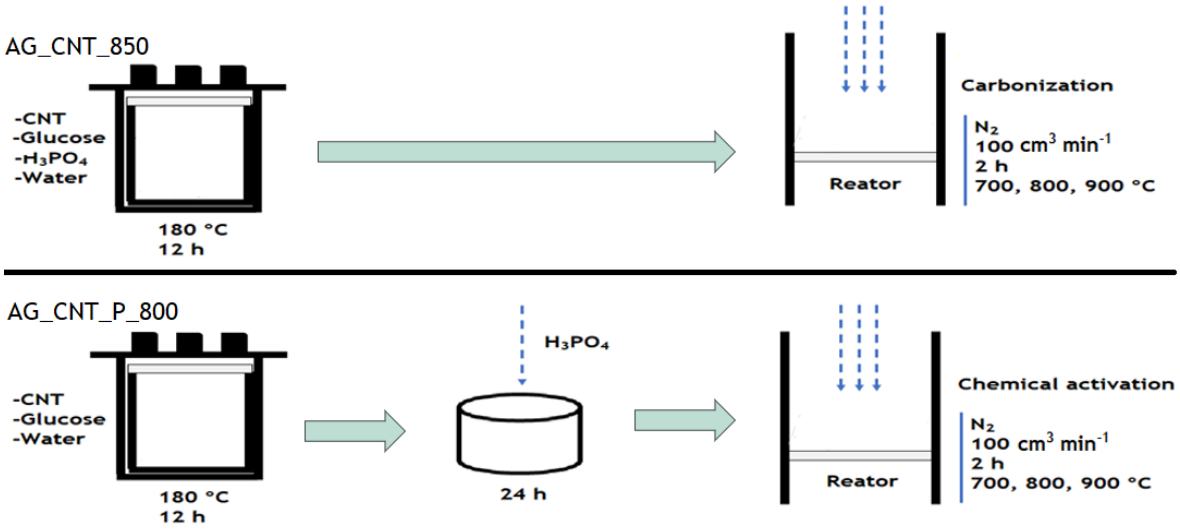

Figure 9 - A schematic representation of the methodology followed for the preparation of activated carbon materials.

3.2 Electrode preparation

All samples were crushed with a mortar and a pestle to obtain small and thin particles. A paste was prepared by mixing 90 wt.% of the carbon material with 10 wt% of a liquid binder, polytetrafluoroethylene (60 wt% dispersion in H_2O) in absolute ethanol. A thin carbon film was formed (Figure 10a), from which the electrodes were punched (Figure 10b). Finally, each electrode was pressed at 5 tonne during 30 s, dried and weighed.

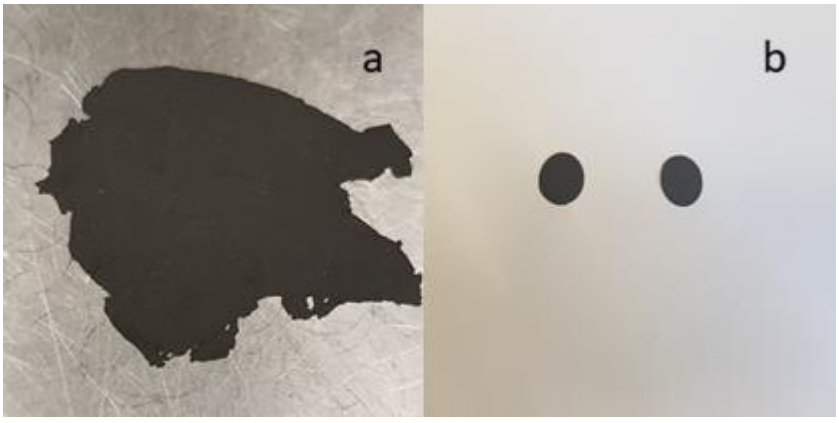

Figure 10 - Carbon material: a - carbon film and b - carbon electrode.

3.3 Cell assembly

Two types of cell configuration were assembly: three-electrode and two-electrode cell configuration.

3.3.1 Three-electrode cell configuration

Three-electrode configuration involves a beaker type cell with three electrodes (working, counter and reference) immersed in 1 M H_2SO_4 electrolyte solution. The working electrode was prepared by sandwiching carbon pellets, with the same are (0.78 cm^2) and similar masses (10 mg), between two stainless steel meshes that were pressed at 5 tonne for 30 s.

Norit DLC Supra 50 was chosen as the counter-electrode and was obtained by the same method as the working electrode but using 20 mg of carbon. An Ag/AgCl (KCl 3 M) electrode was used as a reference electrode. Both working and counter electrodes were separated by filter paper (Whatmann, qualitative filter paper Grade 1) and connected to two metal platinum wires. A scheme of the cell configuration is shown in Figure 11.

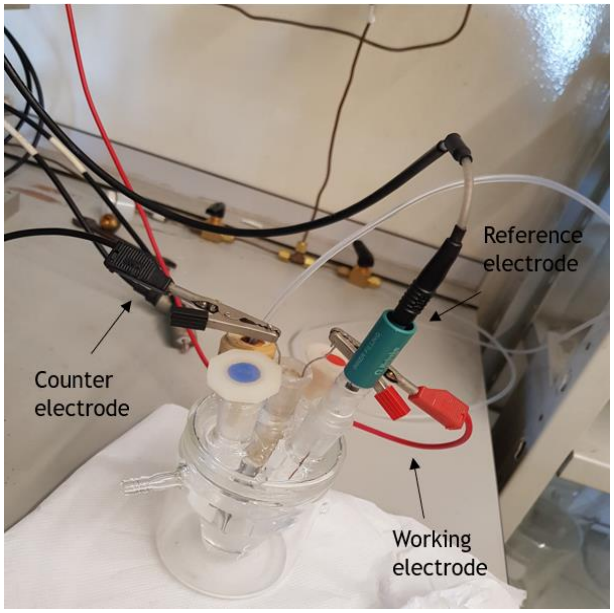

Figure 11 – Three-electrode cell configuration.

3.3.2 Two-electrode cell configuration

In two-electrode cell configuration, two carbon electrodes with similar masses were used as working electrodes, with a separator filter paper (Whatmann ®) in-between and soaked with

the electrolyte solution of 1 M H_2SO_4. The electrodes (2.5 – 6 mg) were stacked between two stainless steel bars, used as current-collectors, which were fixed with a PTFE Swagelok® tube fitting, as shown in Figure 12.

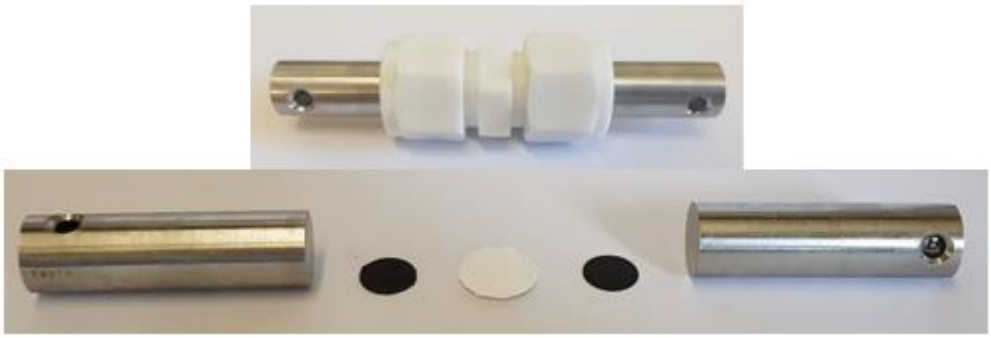

Figure 12 - Supercapacitor cell.

3.4 Materials characterization

3.4.1 Nitrogen adsorption-desorption isotherms

The textural properties of all materials were characterized by analysis of the nitrogen adsorption-desorption isotherms at -196 ºC using a Quantachrome Autosorb iQ automated gas sorption analyzer. Firstly, 100 mg of sample were weighted and loaded in a glass cell, also previously weighted. Afterward, the cells were set in the equipment for degasification under vacuum at 150 ºC for 12 h. The difference between the mass before and after the degasification, was the actual mass of the sample. The specific surface area (S_{BET}) [40] was calculated according to the Brunauer-Emmett-Teller, BET, from the nitrogen adsorption isotherms. The micropore volume, V_{DR}, was calculated by applying the Dubbinin-Radushkevich (DR) method [41]. The total pore volume, V_P, was calculated as the amount of N_2 adsorbed at the saturation pressure and the mesopore volume, V_{meso}, was equal to the subtraction of the total pore volume with the micropore volume.

3.4.2 Scanning electron microscopy

The morphology of the samples was examined with a Quanta FEG 400 (FEI Company) scanning electron microscope, SEM. The analysis was perfomed in Centro de Materiais da Universidade do Porto (CEMUP). The samples were previously attached to an aluminum pin using conductive

double-sided adhesive tape. An accelerating voltage of 15 kV and a secondary electron detector Everhart-Thornley (ETD) were used in all the analyses.

3.4.3 Elemental analysis

The chemical composition of all the samples was determined by elemental analysis, which provides the content of carbon, nitrogen, sulfur and hydrogen in the sample. The analysis was carried out in a Vario Micro Cube analyzer (from Elementar), in which the combustion of the sample at 1050 ºC is forced. Each sample was analyzed in triplicate. Besides one sample of acetanilide (<2 mg) and 3 samples of sulfanilamide (<2 mg), where also prepared and used as standards.

In addition to the traditional elemental analysis performed by combustion of the sample, energy dispersive X-ray spectroscopy, EDS, was also used to characterize the chemical composition of the samples.

The analysis was carried out in a Quanta FEG 400 scanning electron microscope (FEI Company) and was performed in Centro de Materiais da Universidade do Porto (CEMUP). The samples were previously attached to an aluminium pin using conductive double-sided adhesive tape. An accelerating voltage of 15 kV and a secondary electron detector Everhart-Thornley (ETD) were used in all the analyses. This analysis was performed along with the examination of the morphology of the samples.

3.4.4 X-ray photoelectron spectroscopy

X-ray photoelectron spectroscopy, XPS, was used to measure the surface chemical composition of the samples. This technique allows to evaluate the elements that exist, within the first 10 nm of thickness [42], by irradiating the material with X-rays. The analysis was perfomed in Centro de Materiais da Universidade do Porto (CEMUP). The samples were previously attached to a copper foil using a double-sided adhesive tape. Since the carbon powder could not compact in the adhesive tape and could damage the equipment, electrodes were used instead of powder samples in the analysis.

3.4.5 Temperature programmed desorption

The nature and amount of surface oxygenated groups were evaluated by temperature programmed desorption (TPD) carried out in an Altamira Instruments AMI-300 equipment with mass spectrometry detection. 100 mg of sample were weighted and loaded in a glass cell and introduced into the equipment. Each sample was heated at 10 ºC min^{-1} to 1000 ºC in an inert atmosphere. During this treatment, volatile matter is eliminated in the form of CO and CO_2, which are detected in a thermal conductivity detector, TCD.

3.5 Electrochemical measurements

The electrochemical measurements were performed on a PGZ 402 Voltalab potentiostat (Radiometer Analytical) by using the three-electrode and two-electrode cell configuration, described above (see section 3.3). Each configuration was used to study the electrochemical properties and electrochemical performance of each carbon material, respectively. The electrochemical properties of the samples were evaluated by cyclic voltammetry in the three-electrode cell, while the electrochemical performance was evaluated by cyclic voltammetry and galvanostatic charge-discharge methods in the two-electrode cell.

3.5.1 Measurements in a three-electrode cell

Before starting cyclic voltammetry tests in the three-electrode cell, nitrogen was bubbled into the cell to saturate the electrolyte and remove the presence of oxygen. Cyclic voltammetry (CV) tests were carried out in a voltage window of 0.8 V (from -0.2 to 0.6 V) and at various scan rates ranging from (2 to 100 mV s^{-1}). During the CV the current is recorded as a function of the potential applied.

The capacitance (Cs, F g^{-1}) of a single electrode was determined by the following formula:

$$C_s = \frac{1}{rmV_w}\int_{V0}^{V1} I(V)dV \qquad (1)$$

Where *m* is the active mass of the working electrode, *r* is the scan rate (V s^{-1}), *Vw* is the voltage window applied (V) and *I* the measured current (A).

3.5.2 Measurements in a two-electrode cell

The first test performed in the two-electrode cell was the open circuit voltage, OCV, to stabilize the signal. Then cyclic voltammetries were carried out using several voltage windows (0.6, 0.8, 1.0 and 1.2 V) at a constant scan rate of 2 mV s^{-1}.

The capacitance (F g^{-1}) of a single electrode was determined by the following formula:

$$C_s = \frac{2}{rmV_w}\int_{V0}^{V1} I(V)dV \qquad (2)$$

Where *m* is the active mass of the working electrode, *r* is the scan rate ($V.s^{-1}$), *Vw* is the voltage window applied (V) and *I* the measured current (A).

In addition, galvanostatic charge-discharge measurements, CD, were performed at a constant voltage of 0.8 V, at several current density, I, ranging from of (0.1 to 20.0 A g^{-1}).

4 Results and discussion

This chapter discusses the textural and chemical properties of the biomass-derived carbons prepared from the two different methods studied (one-pot and impregnation) and the physically activated samples. The electrochemical performance is also discussed.

4.1 Textural properties

The textual characterization of all materials was performed by nitrogen adsorption/desorption isotherms at -196 ºC. The nitrogen adsorption-desorption isotherm of samples prepared by the one-pot method are shown in Figure 13a, along with the sample CG-CNT, which is a carbonized sample without phosphorous. All the samples exhibit a combination of type I and type IV isotherms that usually corresponds to microporous and mesoporous materials [43]. The isotherms present a large volume of nitrogen adsorbed at low relative pressures, which indicates the presence of a large volume of micropores (Table 4). In addition, the samples exhibit a hysteresis loop that abruptly increase at high relative pressures. This type of hysteresis loop is commonly observed for carbon nanotubes [43]. The micropore volume calculated by Dubbinin-Radushkevich method, ranges from 0.18 to 0.21 $cm^3\ g^{-1}$ and the mesopore volume ranges from 0.10 to 0.12 $cm^3\ g^{-1}$, as shown in Table 4. All one-pot samples present similar surfaces areas, suggesting that the temperature of carbonization does not have significant effect on the specific surface area. However, it should be highlighted that the sample CG_CNT_Pop_800 exhibits higher surface area probably due to the presence of phosphorous during carbonization.

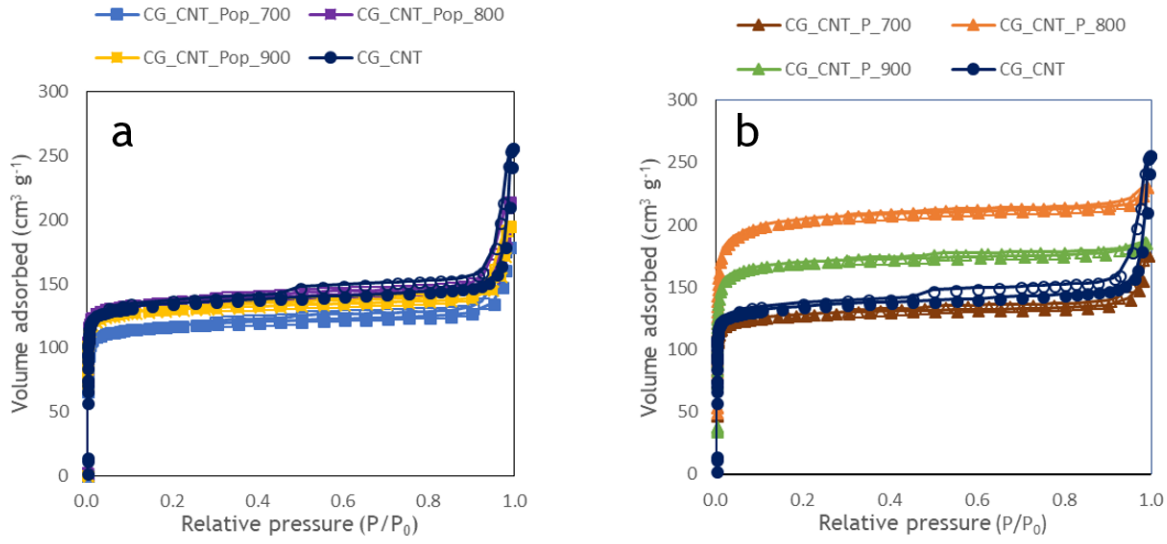

Figure 13 -Nitrogen adsorption/desorption isotherms at -196 ºC of samples prepared by: a - One-pot method and b - Impregnation method.

The nitrogen adsorption/desorption isotherm of samples prepared by the impregnated method are shown in Figure 13b, along with the sample CG-CNT. All impregnated samples exhibit type I isotherm, which is associated with microporous materials. Besides, isotherms show a type H4 hysteresis loop, which indicates the presence of mesopores due to the incorporation of carbon nanotubes [43]. The isotherms present a large volume of nitrogen adsorbed at low relative pressures, which indicates the presence of a large volume of micropores (Table 4). The micropore volume ranges from 0.20 – 0.30 $cm^3\ g^{-1}$, due to the chemical activation by H_3PO_4. The phosphorous doped-carbons prepared by the impregnation method and activated at temperature above 800 ºC display specific surface areas superior to that of the sample without phosphorous (CG_CNT), while sample activated at 700 ºC displays almost the same microporosity. Once again, sample treated at 800 ºC shows the highest specific surface area.

Table 4 - Textural parameters obtained from nitrogen adsorption-desorption isotherms at -196 ºC

Samples	S_{BET} (N_2) ($m^2\ g^{-1}$)	V_{DR} ($cm^3\ g^{-1}$)	V_p ($cm^3\ g^{-1}$)	V_{meso} ($cm^3\ g^{-1}$)
CG_CNT	545	0.22	0.39	0.17
CG_CNT_Pop_700	475	0.18	0.28	0.10
CG_CNT_Pop_800	555	0.21	0.33	0.12
CG_CNT_Pop_900	527	0.20	0.30	0.11
CG_CNT_P_700	521	0.20	0.27	0.08
CG_CNT_P_800	806	0.30	0.36	0.06
CG_CNT_P_900	687	0.26	0.29	0.03
AG_CNT_850	738	0.28	0.30	0.03
AG_CNT_P_800	1452	0.55	0.80	0.25

Figure 14a and b presents the nitrogen adsorption/desorption isotherms at -196 ºC and the corresponding pore size distributions obtained for physical activated carbons, respectively. The activated carbons exhibit type I isotherm, due to the high content of micropore. The observed sharp hysteresis loops reveal very narrow mesopore size distributions. Significant textural changes are observed along this series. When comparing all samples treated at 800 ºC, the physically activated carbon has a higher specific surface area and higher micropore content.

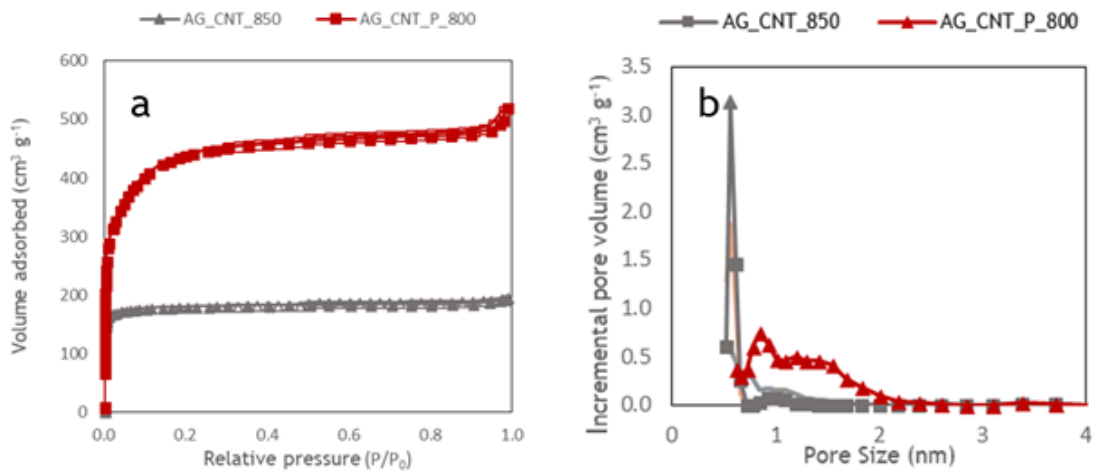

Figure 14 - a - Nitrogen adsorption/desorption isotherms at -196 of and b -pore size distributions of the activated samples.

As previously mentioned, physical activation of the sample modifies the textural properties of the material, as shown in Table 4. The specific area of the activated carbons is greater, due to higher micropore volume. The specific surface areas values are 1452 $m^2 g^{-1}$ and 738 $m^2 g^{-1}$ for AG_CNT_P_800 and AG_CNT_850, respectively.

4.2 Morphological properties

Morphologies of the studied carbon materials were evaluated by using scanning electron microscopy. Figure 15, 16 and 17 show representative SEM image for the carbons prepared by one-pot method, impregnation method and for the physical activated samples, respectively.

Independently of the carbonization temperature, all samples prepared by the one-pot method present similar morphologies, composed of spheres of 5-7 μm (Figure 15). However, this morphology is different than that of sample CG_CNT (Figure 17a), which is composed of spheres of smaller size (approx. 1 μm). This effect can be ascribed to the presence of phosphoric acid during the hydrothermal process, which is modifying the polymerization reaction of glucose, giving rise to sphere of larger size.

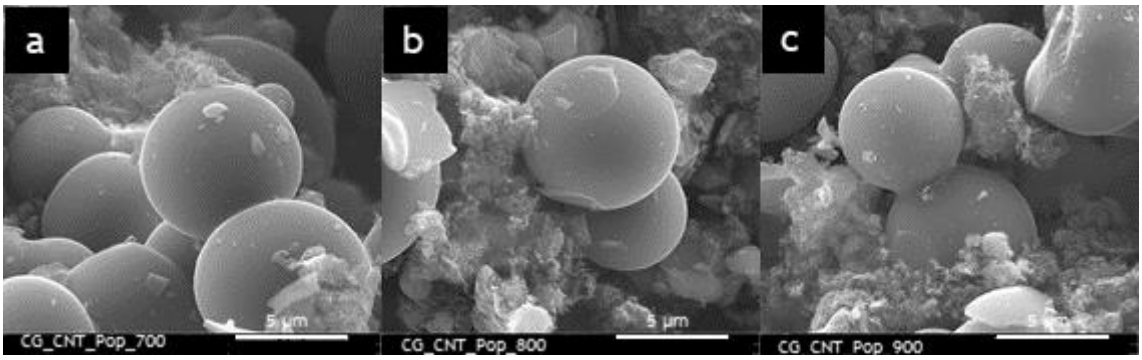

Figure 15 – SEM images of one-pot samples.

In the other hand, there is also visible changes between the samples prepared by the impregnation method shown in Figure 16 and sample CG_CNT shown in Figure 17a. These differences indicate that the thermal treatment is altering the morphology of the samples. These samples were impregnated with phosphoric acid prior to the thermal treatment, so the acid acted as activating agent. During activation reaction part of the solid material is removed, leading to spheres of smaller size and to a more compact structure.

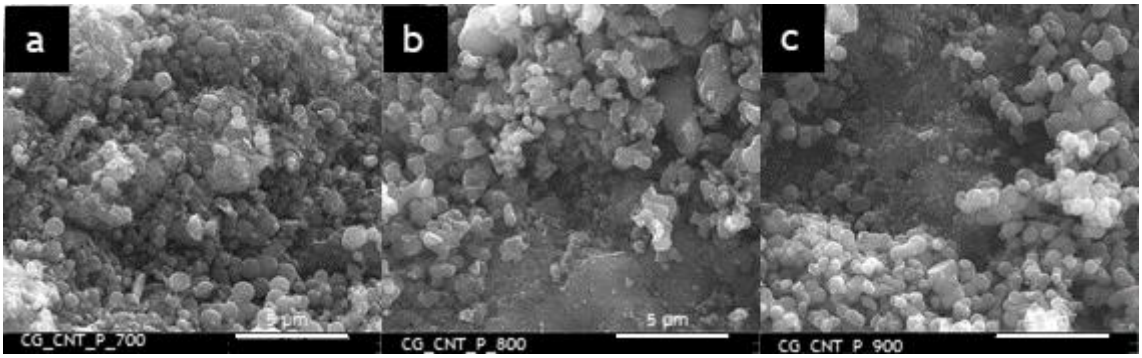

Figure 16 - SEM images of impregnated samples.

SEM images for the physical activated carbons with and without phosphorous are shown in Figure 17b and 17c, respectively. The sphere size of the physical activated is similar to that of chemical activated samples (impregnated samples). Suggesting that the size of the spheres is due to activation and not to the presence of phosphoric acid. However, the spheres from the physically activated samples show an irregular shape.

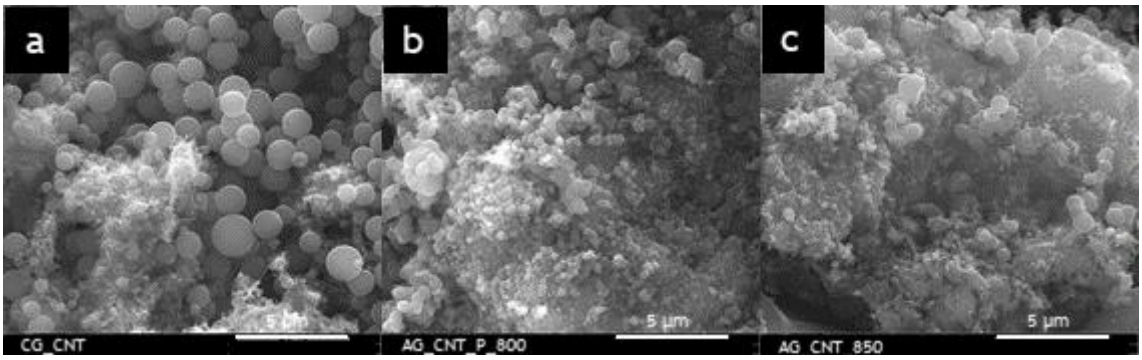

Figure 17 – SEM images of: a- CG_CNT, b – AG_CNT_P_800 and c – AG_CNT_850.

For a better understating of the morphologies SEM images took at different scales are shown in Appendix A.

4.3 Chemical properties

An elemental analysis, EA, was made to evaluate the composition of carbon, hydrogen, nitrogen and sulfur of the prepared materials. The content of oxygen and phosphorus was analyzed by energy dispersive X-ray spectroscopy (EDS). All values obtained are shown in table 5. All the samples are composed mainly of carbon, with contents ranging from 75 % to 94 %. As expected, no nitrogen and sulfur are present in the samples.

The quantity of hydrogen in the samples prepared by one-pot method decreases as the temperature of carbonization increases, while by the impregnated method, the sample CG_CNT_P_800 presents the highest hydrogen content. This is possibly due to a higher phosphorous content. This effect is also notable between the physical activated samples, where the sample with more phosphorous has higher hydrogen content.

Table 5 - Elemental composition (wt. %) obtained from elemental analysis and energy dispersive X-ray spectroscopy

Samples	Elemental Analysis (wt. %)					EDS (wt. %)	
	C (%)	H (%)	N (%)	S (%)	Diff (%)	O (%)	P (%)
CG_CNT	93.8	1.6	0.0	0.0	4.6	4.6	0.0
CG_CNT_Pop_700	91.2	1.2	0.0	0.0	7.6	7.0	0.6
CG_CNT_Pop_800	88.9	0.8	0.0	0.0	10.3	8.6	1.7
CG_CNT_Pop_900	91.3	0.5	0.0	0.0	8.2	7.6	0.6
CG_CNT_P_700	88.4	1.3	0.0	0.0	10.3	8.0	2.3
CG_CNT_P_800	75.3	1.8	0.0	0.0	22.9	12.6	10.3
CG_CNT_P_900	83.0	1.0	0.0	0.0	16.0	9.0	7.0
AG_CNT_P_800	87.4	0.7	0.0	0.0	11.9	7.6	4.3
AG_CNT_850	94.3	0.4	0.0	0.0	5.3	5.3	0.0

The values obtained from EDS analysis, corresponding to the content of oxygen and phosphorous, are also plotted in Figure 18 to a better understanding on how the content of oxygen and phosphorus evolve with temperature for the two different methods used to prepare the samples. It seems that the impregnation method increases the amount of oxygen and phosphorous into the carbon structure when compared with the one-pot method.

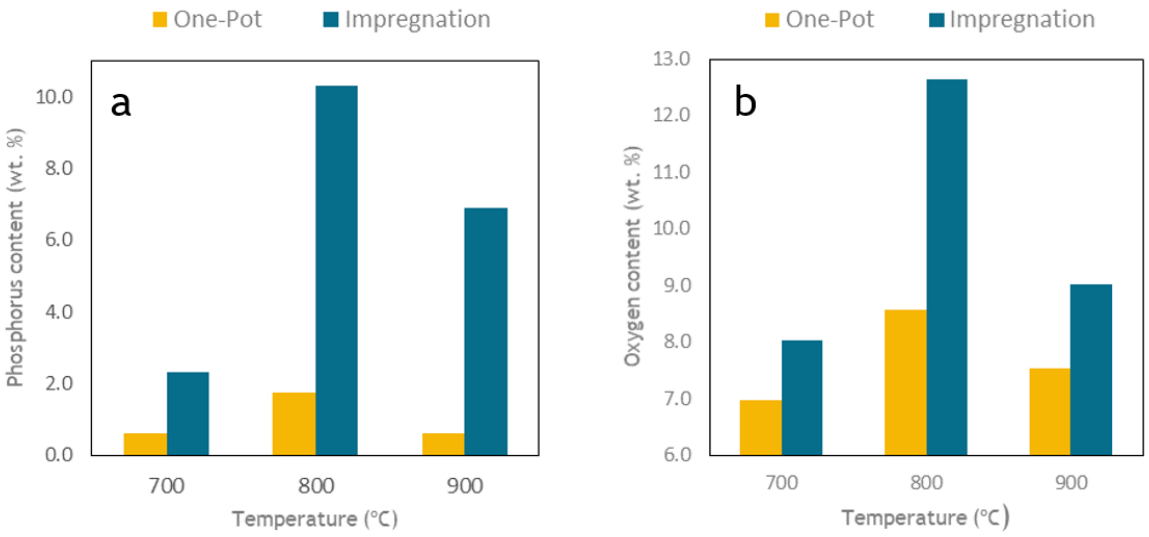

Figure 18 – a - phosphorus content and b – oxygen content provided by EDS.

It is also notable for both methods that, the phosphorus content increases up to 800 ºC reaching a level of about 10.3 wt. % and 1.7 wt. % for samples CG_CNT_P_800 and CG_CNT_Pop_800,

respectively. The oxygen content exhibits a similar trend as the phosphorous, suggesting that the oxygen is being introduce from the phosphoric acid.

It should be highlighted that the oxygen and phosphorus content for sample AG_CNT_P_800 are lower that for sample CG_CNT_P_800 sample, probably due to the higher time of activation used, 4 h instead of the 2 h employed for sample CG_CNT_P_800.

XPS is a surface technique that was conducted to study and understand the differences on the surface functionalities originated from the incorporation of the phosphoric acid. The XPS spectrum indicates the presence of three distinct peaks attributed to carbon, oxygen and phosphorus. The carbon region C 1s and oxygen region O 1s, for all samples are shown in Figure 19.

All samples present a XPS spectra for the C 1s region with two peaks. The first peak at around 285 eV. The second odd peak is due to the presence of Fluor bonds from the liquid binder, since the material analyzed was the electrode instead of the powder.

All samples present in the O 1s region one broad peak centered at 532 eV, that can be assigned to different functional oxygen groups [44]. In this case since, phosphorous is present in all samples, it is difficult to distinguish organic oxygen present in carboxyl, carbonyl, alkoxyl or ether groups from inorganic oxygen present in phosphates [44].

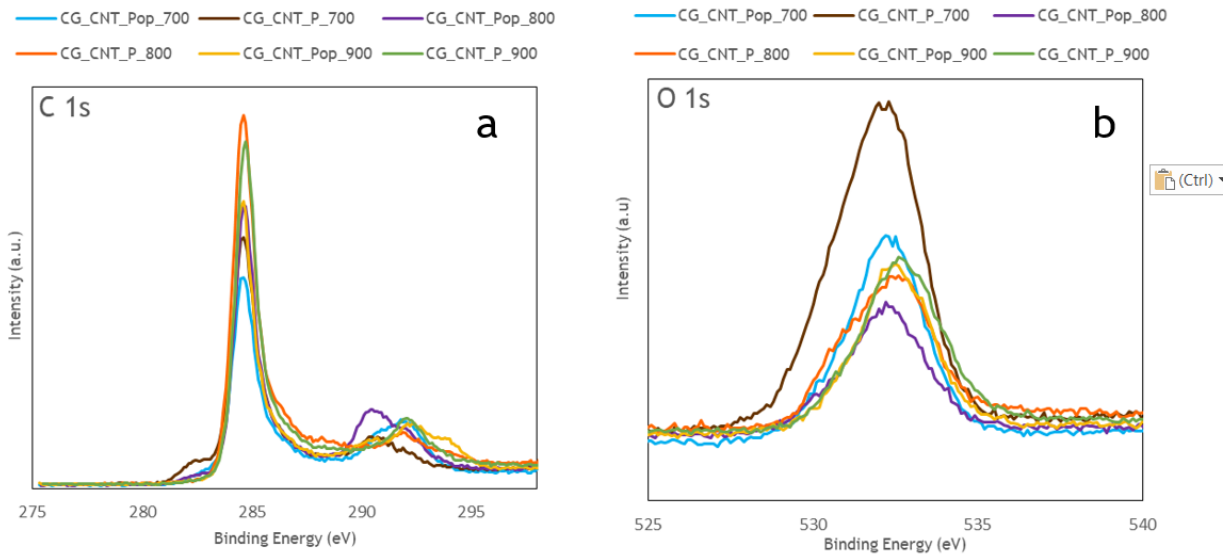

Figure 19 - X-ray photoelectron spectrum of C 1s and O 1s regions for phosphorus doped carbons .

It is noteworthy high percentages of oxygen in CG_CNT_P_700, because XPS analysis only determines the content in the surface of the sample and maybe that is the reason why the content of oxygen provided by XPS is not in agreement with that of EDS. The same effect occurs with the sample CG_CNT_Pop_700, which has the second highest oxygen content, accordingly to XPS.

The phosphorus region, P(2p) between 128 – 140 eV is represented in Figure 20 for all samples prepared by the two doping methods.

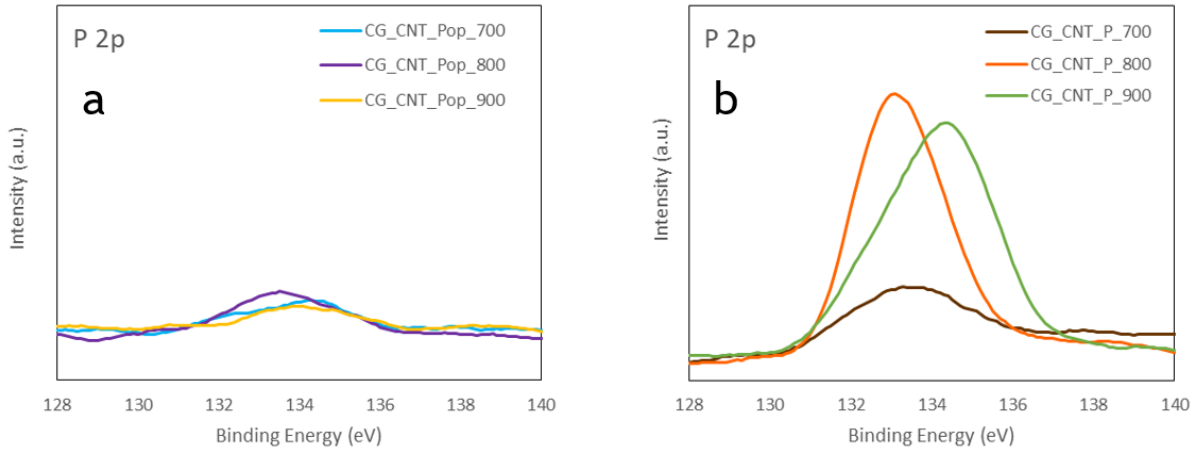

Figure 20 - X-ray photoelectron spectrum of P 2p regions for: a- one-pot samples and b - impregnated samples.

Analyzing P2p region, it can be verified that the data from the XPS is in agreement with the data provided from the EDS, in terms of phosphorous content. All impregnated samples exhibit higher content of phosphorus than samples prepared by one-pot method. Moreover, interesting differences are also observed for impregnated samples. In order to study these differences in more detail, the deconvolution of the peaks in the P2p region was performed for all impregnated samples (Figure 21). The position and FWHM of the different peaks obtained from the deconvolutions are shown in Table 6.

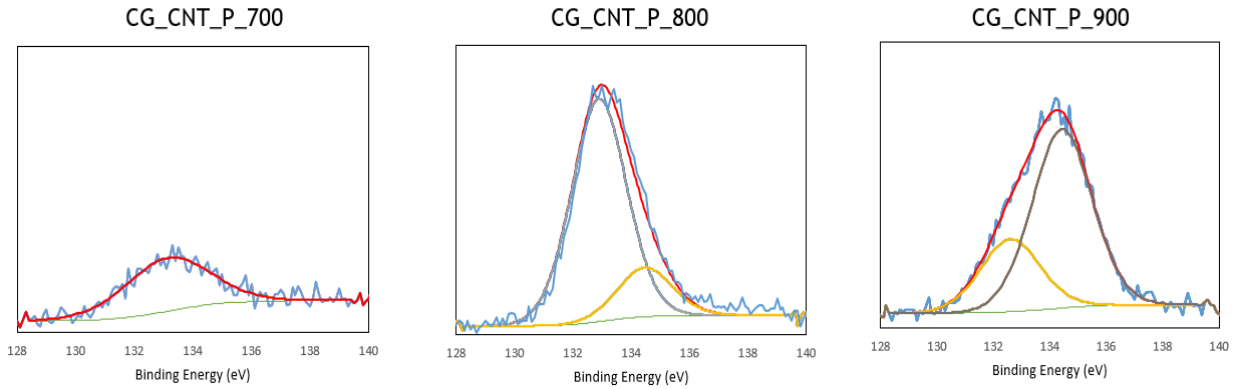

Figure 21 - Deconvoluted P 2p region for impregnated samples.

The main component of CG_CNT_P_700 represents almost the 100 % of the overall contribution and corresponds to phosphate group, while in samples, CG_CNT_P_800 and CG_CNT_P_900, the peak can be deconvoluted into two components: phosphates and metaphosphates.

It is noteworthy that phosphate peak is shifted to lower binding energy as the activation temperature increased from 700 to 900 ºC. This can be justified by two reasons: i) gradual dehydration and condensation of phosphoric acid into polyphosphates and ii) interaction of phosphorus with enlarged aromatic carbon ring system (BE = 132.6 eV) [44]. There is also an increase of metaphosphates with a temperature increase. The impregnated sample treated at 900 ºC has higher content of metaphosphates groups while the impregnated sample treated at 800 ºC has higher content of phosphate groups, as shown in Figure 21.

Table 6 - Deconvolution results of XPS spectra for impregnated samples

Region	**CG_CNT_P_700**		**CG_CNT_P_800**		**CG_CNT_P_900**		**Functional groups**
	Position (eV)	Quantity (%)	Position (eV)	Quantity (%)	Position (eV)	Quantity (%)	
P2p	133.1	100	132.9	82.0	132.6	28.9	Phosphates
	-	-	134.5	18.0	134.4	71.1	Metaphosphates

The most prevalent functional group is phosphate, where phosphorus is bound to 4 oxygen atoms in a tetrahedral configuration. This is in line with the study done by A.M. Puziy et al, who conclude that for high carbonization temperatures the most common bond is C-O-P over C-P-O, showing greater thermal stability, as the most abundant phosphorous species between 400 – 1000 ºC was phosphate [44].

The nature of the oxygen-containing functionalities was analysed by temperature programmed desorption experiments. The decomposition of oxygen groups upon heating, releases CO and CO_2 at certain temperatures. The total amount of CO_2 can be assigned to carboxylic acids, anhydrides, and lactones, while the release of CO corresponds to anhydrides, phenols and carbonyl/quinone groups [26]. The CO_2 and CO desorption profiles for all prepared carbons are shown in Figure 22.

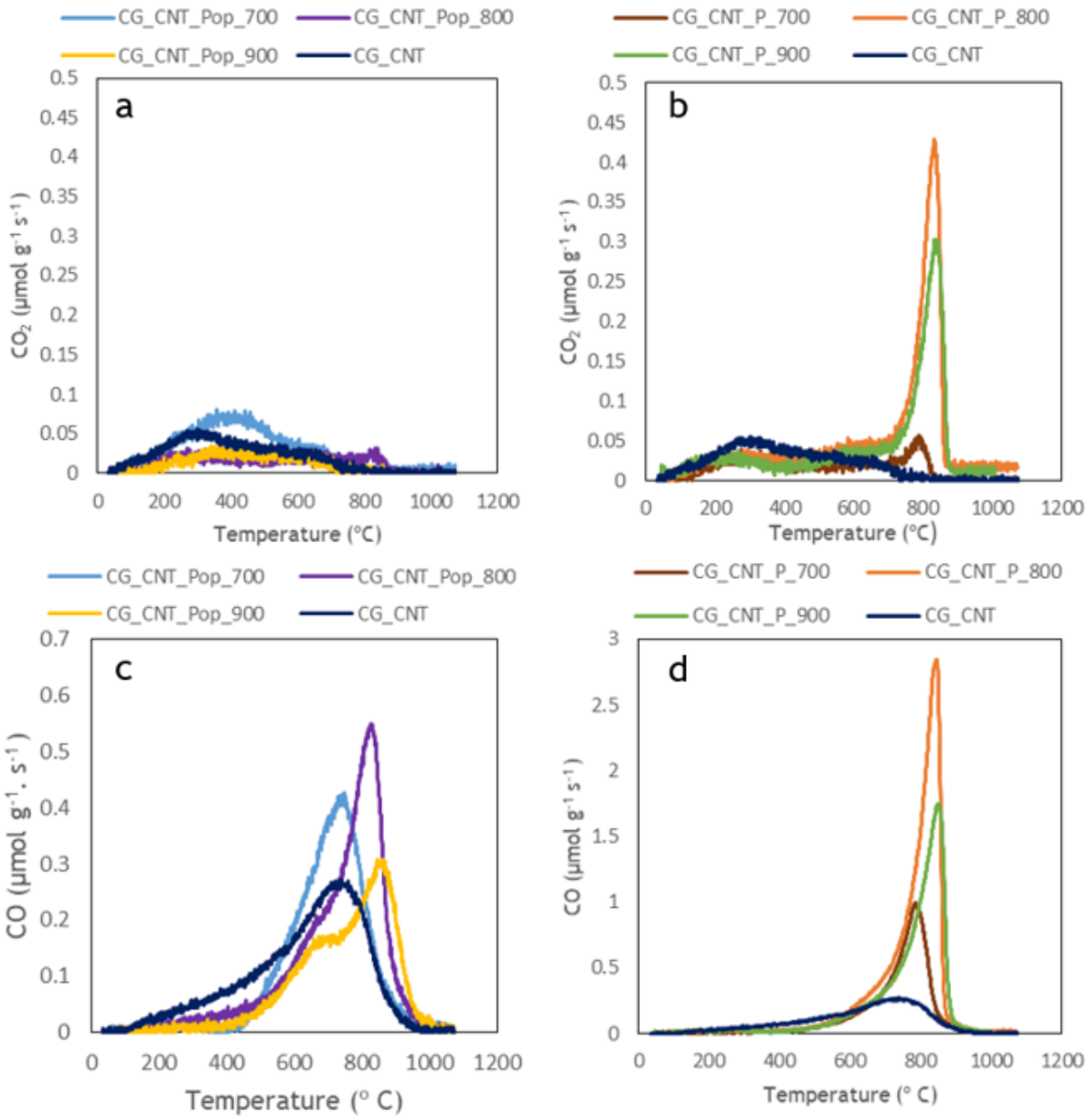

Figure 22 - TPD spectra of: a - one-pot CO_2, b - impregnation CO_2, c - one-pot CO and d-impregnation CO.

The sample CG_CNT exhibits two distinctive broad peaks in the CO_2 spectra centered at 300 ºC, and at 600 ºC, respectively, which are associated with carboxylic anhydrides and carboxylic anhydrides groups [26]. CG_CNT_Pop_700 exhibit similar peaks, but higher amount of CO_2 is released. Samples CG_CNT_Pop_800 and CG_CNT_Pop_900 show similar CO_2 peaks than CG_CNT, even the quantity of carboxylic acid decreases by increasing the temperature of carbonization.

Regarding the CO profile, two main peaks can be identified in sample CG_CNT (Figure 22c). The first peak, centred at 600 ºC, is attributed to carboxylic anhydride groups [26]. The last peak appears in an interval temperature of 550 – 900 ºC, which corresponds to phenols and carbonyl quinone groups. Samples prepared by the one-pot method do not exhibit the peak attributed to strong carboxylic acids, as all the CO_2 is released at temperatures higher than 400 ºC. CG_CNT_Pop_700 show a similar curve than sample CG_CNT, but with higher quantity of CO released, suggesting a higher oxygen content, which is in agreement with EDS results shown in Table 5. Samples CG_CNT_Pop_800 and CG_CNT_Pop_900 show an increase of the CO released at higher temperature, suggesting a lower contribution of phenols and a higher contribution of carbonyl quinone groups [22].

The CO_2 profile of the samples obtained by the impregnation method display two broad peaks centered at 300 ºC and 600 ºC, which, as in the case of the one-pot series, indicates the presence of carboxylic acid and anhydride groups (Figure 22b). Interestingly, these samples also display an unusual sharp peak at 800 ºC. This last sharp peak could probably be related to cleavage of C–O–PO_3 groups related to the phosphate and metaphosphate groups. It should be noticed that sample CG_CNT_P_800 shows the highest peak at 800 ºC, which is indicative of the higher amount of phosphorus. These results are in agreement with those obtained by EDS and XPS.

The three samples obtained by the impregnation method exhibit three peaks in the CO profile. The first peaks is similar to that on sample CG_CNT, which corresponds to carboxylic anhydride groups. In addition, a sharp peak appears at around 830 ºC, which can be attributed to carbonyl quinones groups and the presence of phosphorus groups [45]. Sample CG_CNT_P_800 shows a more intense peak due to its higher content of phosphorus

The temperature programmed desorption experiments were also performed for the activated samples. Figure 23 shows the CO and CO_2 profiles obtained for the activated samples. Samples CG_CNT_P_800 was also added for comparison purpose.

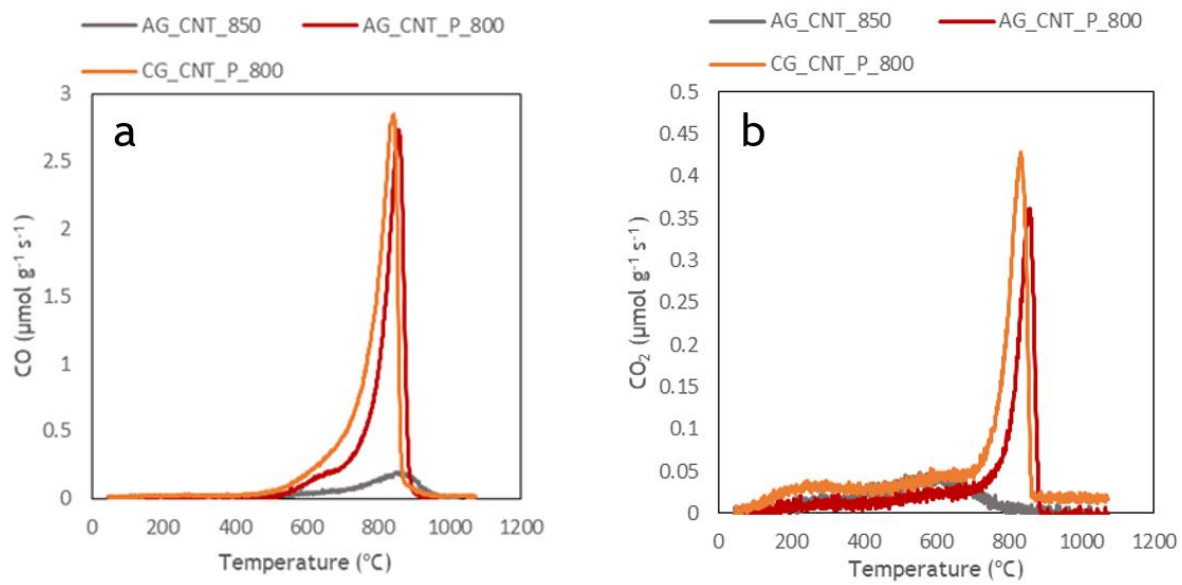

Figure 23 - TPD spectra of activated samples: a- CO profile and b-CO_2 profile.

Regarding the CO_2 profile of the samples obtained by physical activation, it does not present the same amount of carboxylic acid, since they were treated with a different atmosphere, and originated different oxygen groups. The samples that contain phosphorous have a peak at 800 ºC.

The CO profile, for all samples, exhibits a peak at 800 ° C associated with carbonyl/quinones, although the sample without phosphorous has a lower contribution. The peak around 800 ºC is higher in the samples that contain phosphorous due to the presence of phosphorous bonds, as previously mentioned.

The data from the TPD, is in agreement with the EDS results shown in Table 5. The impregnation method exhibits higher oxygen content, which in this case is reflected by the higher amount of CO and CO_2 released.

4.4 Electrochemical measurements

Different electrochemical measurements were performed for all the prepared carbons. The first test was performed in a three-electrode cell, in order to evaluate the electrochemical performance and the rest of the testes were performed in a two-electrode cell to evaluate the supercapacitor performance. A commercial activated carbon, Norit DLC Supra 50, was also tested for comparison purposes.

4.4.1 Electrochemical performance

Cyclic voltammetry (CV) tests carried out in a voltage window of 0.8 V (from -0.2 to 0.6 V) and at a scan rate of 2 mV s^{-1} are shown in Figure 24. All the voltammograms were expressed as capacitance (F g^{-1}) versus voltage (V). The specific capacitance was calculated using equation 1 (see section 3.5.1) and the values obtained are listed in Table 7, along with the BET surface area and the content of oxygen and phosphorous (results previously discussed).

The cyclic voltammetries of samples prepared by the one-pot method are shown in Figure 24a, along with the results of sample CG_CNT. All one-pot samples exhibit a non-square shape cyclic voltammetry which is similar to that of carbonized sample CG_CNT. This effect is expected, since all samples present similar surface areas. Sample CG_CNT_Pop_800 presents the most rectangular shape and hence, the highest capacitance probably due to the higher amount of oxygen and phosphorous, as shown in Table 7.

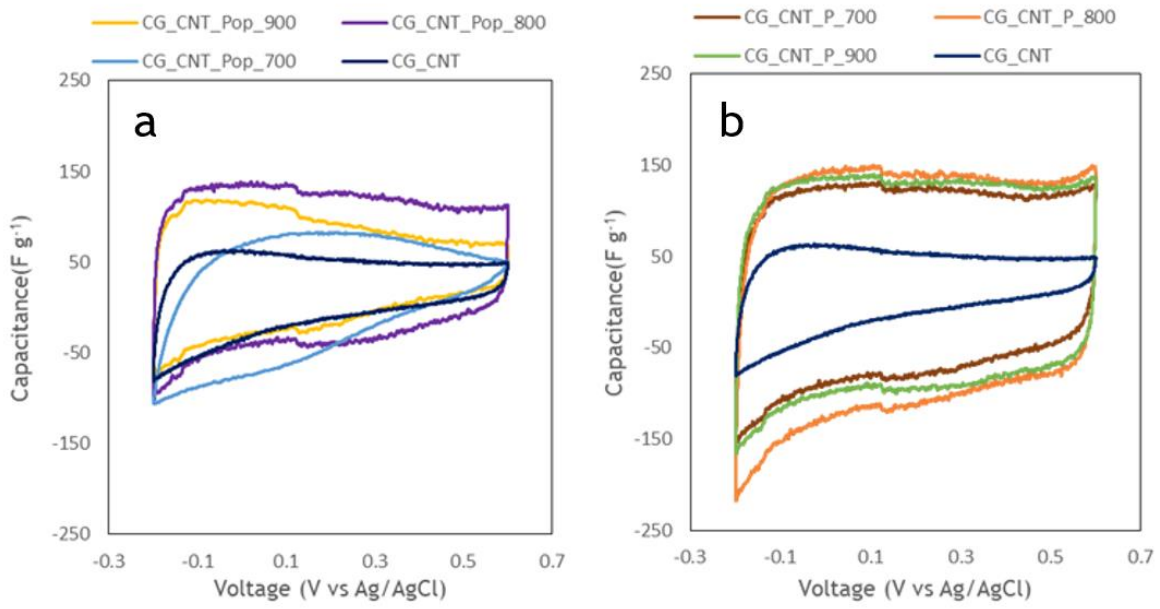

Figure 24 - Cyclic voltammetries at scan rate of 2 mV s^{-1} for: a - One-pot samples and b - impregnated samples

The cyclic voltammetries of samples prepared by the impregnation method are shown in Figure 24b, along with the sample CG_CNT. All studied impregnated samples present CVs with more rectangular shape than the carbonized samples, indicating a better capacitive response. As shown in Table 7, the capacitance of sample CG_CNT_P_700 is higher than that of sample CG_CNT, despite of having a similar surface area, and double of that of sample CG_CNT_Pop_700, which shows slightly lower surface area and similar oxygen content. Accordingly, it can be inferred that this effect is probably due to the phosphate groups present on the surface of sample CG-CNT_P_700.

CG_CNT_P_800 displays the highest capacitance of the three impregnated samples, probably due to the combination of the highest surface area with the highest content of oxygenate and phosphate groups. It should be noted that although sample CG_CNT_P_900 has higher surface area and higher degree of functionalization than sample CG_CNT_P_700, the capacitance obtained are quite similar. These results suggest that the type of phosphorous group is also playing an important role on the final capacitance. Sample activated at 900 ºC exhibit a larger contribution of metaphosphates, while sample CG_CNT_P_700 showed a higher contribution of phosphate, which seems to favor the formation of the EDL.

Table 7 - Capacitance calculated the cyclic voltammetries obtain from three-electrode configuration, BET surface area and oxygen and phosphorous compositions

Sample	**Voltammetry**	S_{BET}	**EDS (wt%)**	
	Cs ($F\ g^{-1}$)	($m^2\ g^{-1}$)	O [%]	P [%]
CG_CNT	32	545	4.6	0.0
CG_CNT_Pop_700	49	475	7.0	0.6
CG_CNT_Pop_800	77	555	8.6	1.7
CG_CNT_Pop_900	53	527	7.6	0.6
CG_CNT_P_700	96	521	8.0	2.3
CG_CNT_P_800	120	806	12.6	10.3
CG_CNT_P_900	108	687	9.0	6.9
AG_CNT_850	103	738	5.3	0
AG_CNT_P_800	118	1452	7.6	4.3

Changes on the micropore volume and modification of the surface groups have a direct effect on the capacitance. In order to evaluate these effects in more detail, cyclic voltammetries of activated samples, with and without phosphorus were performed. The results obtained are shown in Figure 25.

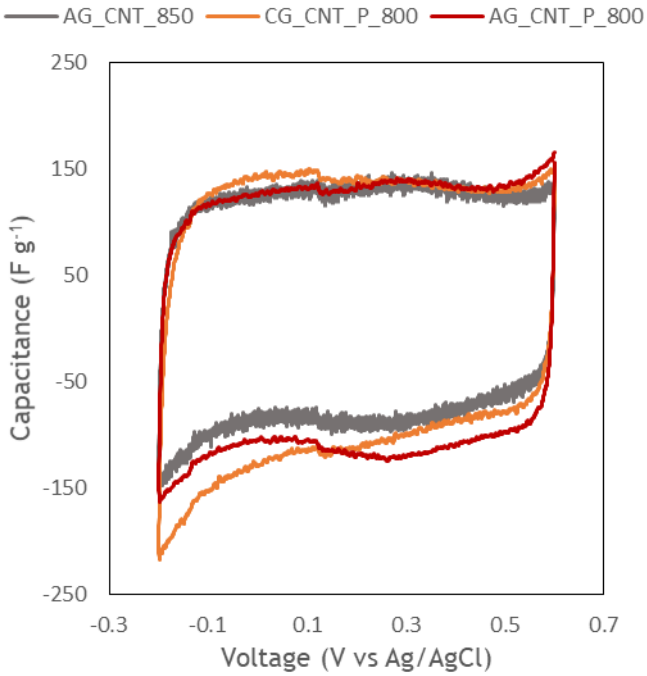

Figure 25 - Cyclic voltammetry at scan rate of 2 mV s^{-1} for physical activated samples and CG_CNT_P_800

Figure 25 was made to compare the best impregnated sample, with one sample without phosphorus, but with similar micropore volume and a physically activated phosphorus sample.

The physical activated samples exhibit anodic and cathodic peaks at around 0.3 V vs Ag/AgCl (KCl, 3 M), which, in carbon materials, is generally associated with the quinone-hydroquinone redox couple. These results are in agreement with those obtained by TPD in which a peak in the CO profile attributed to the quinone groups was observed for both samples.

The sample AG_CNT_P_800 has a larger surface area than sample CG_CNT_P_800 but exhibit similar capacitance. This result reinforces the hypothesis proposed: higher content of phosphate groups improves the capacitance of the carbon material in a three-electrode cell configuration.

4.4.2 Supercapacitor performance

The supercapacitor performance was evaluated in a two-electrode cell. One of the most desirable feature in a supercapacitor is the capacitance. Devices that have higher capacitance are able to store large quantities of energy. Cyclic voltammetry (CV) tests carried out in a voltage window of 0.8 V and at a scan rate of 2 mV s^{-1} are shown in Figure 26. All the voltammograms were expressed as capacitance (F g^{-1}) versus voltage (V). The values for specific

capacitance were calculated using equation 2 (see section 3.5.2) and the values obtained are listed in Table 8. The CVs obtained at different potentials for CG_CNT_Pop_800 and CG_CNT_P_800 are shown in appendix C.

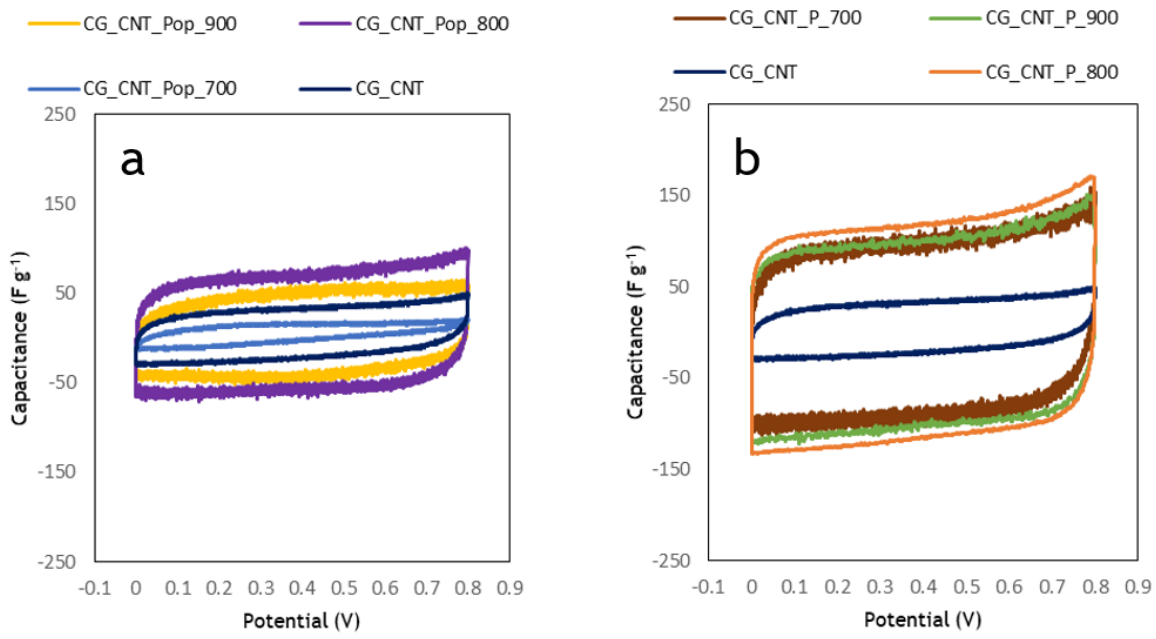

Figure 26 - Cyclic voltammeties at the scan rate of 2 mV s^{-1} and 0.8 V for: a - one-pot samples and b - impregnated samples

Table 8 – Capacitance values calculated from the cyclic voltammetries obtain from two-electrode configuration, BET surface area and oxygen and phosphorous compositions

Sample	Voltammetry	S_{BET}	EDS (wt%)	
	Cs (F g^{-1})	($m^2.g^{-1}$)	O [%]	P [%]
CG_CNT	26	545	4.6	0.0
CG_CNT_Pop_700	8	475	7.0	0.6
CG_CNT_Pop_800	62	555	8.6	1.7
CG_CNT_Pop_900	42	527	7.6	0.6
CG_CNT_P_700	92	521	8.0	2.3
CG_CNT_P_800	116	806	12.6	10.3
CG_CNT_P_900	101	687	9.0	7.0
AG_CNT_P_800	133	738	7.6	4.3
AG_CNT_850	89	1452	5.3	0.0
Supra	120	1961	-	-

The capacitance values in two electrode cells are lower than those obtained in the three-electrode cell configuration, since the presence of redox reactions (Faradaic reactions) are less

evident in the two-electrode configuration. This effect is also confirmed by the more rectangular shape obtained for the cyclic voltametries, which is even more evident for one-pot sample.

CG_CNT shows a distorted CV curve, that indicates a higher resistance. CG_CNT_Pop_700 exhibit lower capacitance, than CG_CNT, since it has lower specific surface area. This effect was not shown in the CVs obtained in the three-electrode cell configuration in which sample CG_CNT_Pop_700 had higher capacitance than CG_CNT. This phenomenon is due to the effect of the pseudocapacitance shown in Figure 26a that lead to a higher total capacitance (49 and 8 F g^{-1} for three and two-electrode configuration, respectively). Sample CG_CNT_Pop_800 presents the highest specific capacitance (62 F g^{-1}) due to the higher amount of phosphorous functionalities.

CVs of samples prepared by impregnation method at scan rate of 2 mV s^{-1} at a potential of 0.8 V, are shown in Figure 26b. All impregnated samples present rectangular shape CV curves, evidencing a better conductivity and an electrical double layer capacitor behavior. The capacitance of the samples increases with the value of the surface area and the amount of phosphorous.

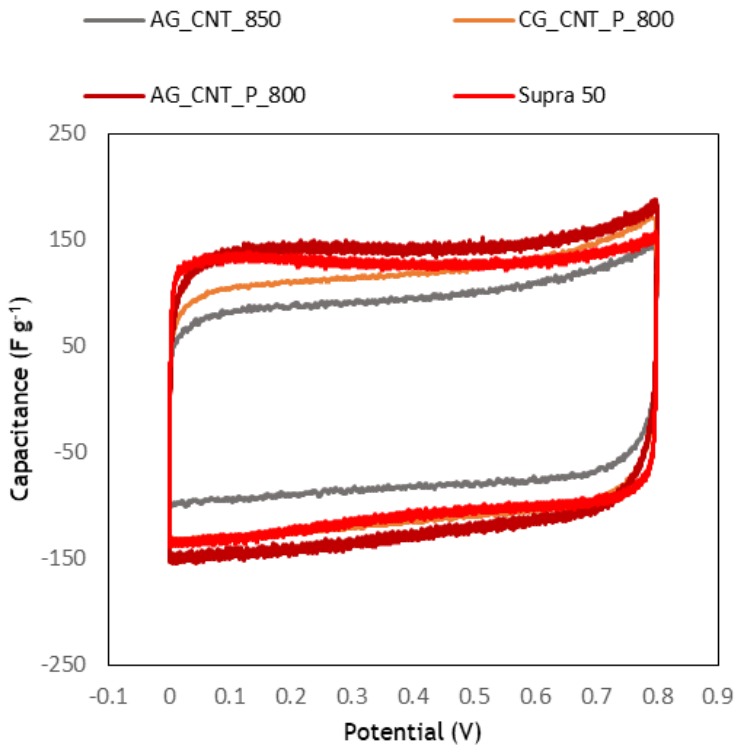

Figure 27 - Cyclic voltammetries at the scan rate 2 mV s^{-1} and 0.8 V of physical activated samples, CG_CNT_P_800 and Supra 50

Cyclic voltammetries of samples physically activated are shown in Figure 27, along with a reference carbon, Supra 50 and sample CG_CNT_P_800. Sample AG_CNT_850 shows a similar CV curve than that of sample CG_CNT_P_800 but 23 % less capacitance despite of showing a similar surface area. This result is, once again, demonstranting the important role that phosphours is playing on the supercapacitor performance. Comparing AG_CNT_P_800 with CG_CNT_P_800, the physical activated sample has a more rectangular shape of the curve and an improved specific capacitance (133 F g^{-1}). In fact, the supercapacitor performance of AG_CNT_P_800 is similar to that of the reference material, despite having lower specific surface area.

The galvanostatic charge/discharge was the second test performed, to evaluate the response of the electrodes. Figure 28a shows the galvanostatic charge/discharge measurements at 0.2 A g^{-1} for one-pot samples and CG_CNT, which results are in agreement with those obtained from CV. The resulting charge/discharge profiles at 0.2 A g^{-1} have a linear shape, which indicates a good capacitance response. At 0.8 V the sample CG_CNT_Pop_800 can store more energy, proving a better capacitance over the other one-pot samples, due to higher surface area and higher oxygen and phosphorous content.

Figure 28b shows the galvanostatic charge/discharge measurements at 0.2 A g^{-1} for impregnated samples. All impregnated samples show better capacitance relative to CG_CNT, since all impregnated samples have a broader charge/discharge curve. The sample CG_CNT_P_800 has the best capacitance, since it has higher surface area and higher oxygen and phosphorous content.

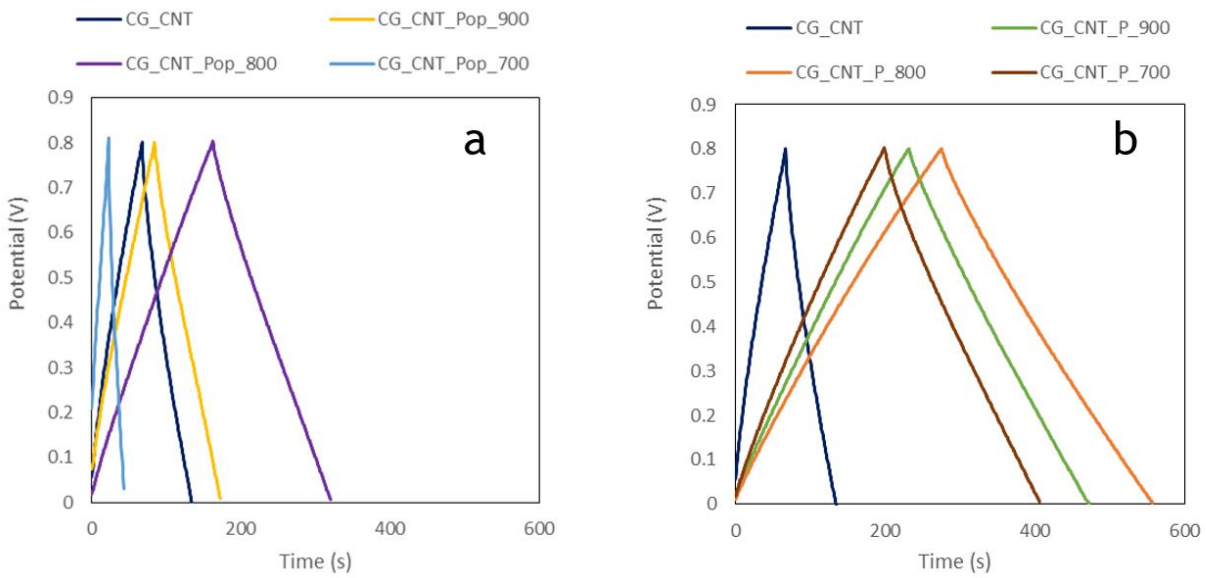

Figure 28 – Galvanostatic charge and discharge for: a - one-pot samples and b – impregnated samples

The galvanostatic charge/discharge measurements for the physical activated samples and the reference material (Supra 50) are shown in Figure 29.

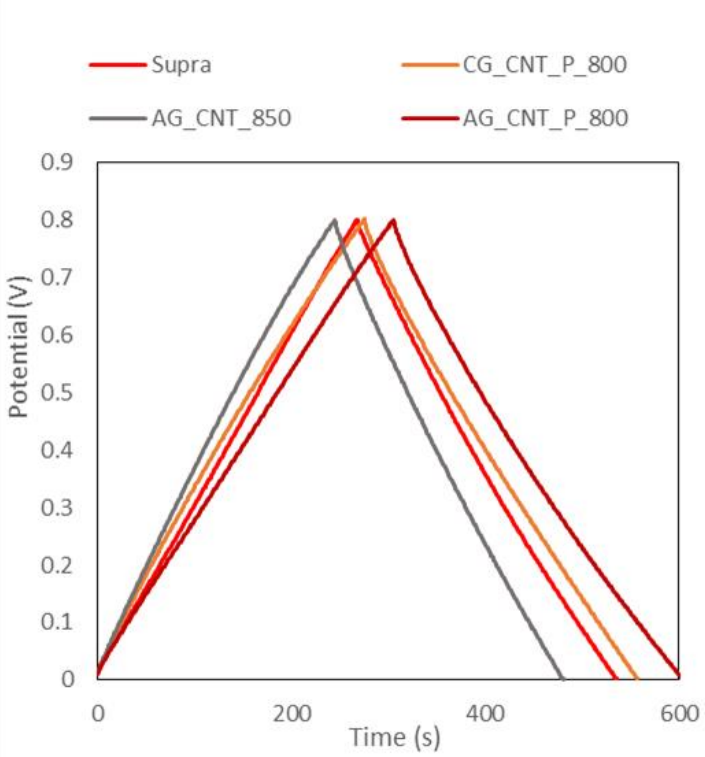

Figure 29 - Galvanostatic charge and discharge for activated samples and Supra 50

Comparing the two samples that have similar surface area (CG_CNT_P_800 and AG_CNT_850) it is noticeable that the sample that contains phosphorous displays higher capacitance, which

means that phosphorous is improving the overall supercapacitor performance. The results show that AG_CNT_P_800 present the best capacitance, since it combines a good content of phoshporous and a higher specific surface area.

The relationship between the specific capacitance and the current density was also evaluated and the results obtained are shown in Figure 30. The galvanostatic charge and discharge results collected at different current densities (0.1 to 10 A g^{-1}) are shown in Appendix D. All the electrodes suffer a decrease in the capacitance when increasing the current density.

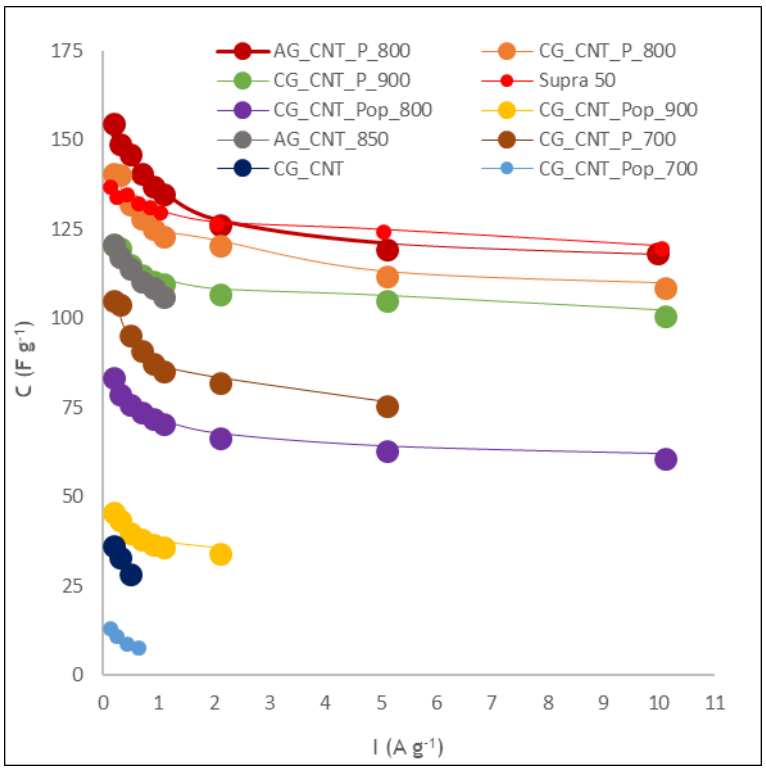

Figure 30 - Evolution of the specific capacitance with current load from 0.1 to 10 A g^{-1}

Carbonized sample (CG_CNT) and one-pot samples cannot support high current densities, higher than 2 A g^{-1}. The only one-pot sample that sustained a current density of 10 A g^{-1} was CG_CNT_Pop_800. In fact, this sample showed a good capacity retention (73.3 %) from 0.1 A g^{-1} to 10 A g^{-1}.

Impregnated samples show high capacitance retention (77.5 % and 84.0 % for samples CG_CNT_P_800 and CG_CNT_P_900, respectively). The sample CG_CNT_P_700 could not support a current density of 10 A g^{-1} but showed a capacity retention of 72.2 % from 0.1 A g^{-1} to 5 A g^{-1}.

The physical activated sample containing phosphorous presents the highest specific capacitance at 0.1 A g^{-1} and a capacitance retention of 75.4 %, showing a capacitance at 10 A g^{-1} similar to that of the reference material (118 F g^{-1}).

5 Conclusion

Functionalized carbon materials derived from biomass with tailored porous and chemical properties were prepared. In addition, the electrochemical performance of the prepared materials was evaluated and a relationship between the textural and chemical properties with the electrochemical performance of the materials was stablished.

The phosphorous doped carbon materials were prepared by two different methods (one-pot and impregnation) and subsequent thermal treated at three different temperatures. The texture and chemical properties are strongly dependent on the preparation method and the carbonization temperature. Impregnated samples resulted in higher specific surface areas and higher oxygen and phosphorous content. In fact, it was demonstrated that the formation and type of phosphorous containing groups are strongly temperature-dependent. The maximum number of phosphorous groups and highest surface area were obtained for the samples treated at 800 ºC. In addition, two more sample were also prepared by physical activation, resulting in materials with an enhanced textural structure.

Electrochemical tests were performed in three and two-electrode cells to evaluate the performance of the biomass-derived carbons prepared in supercapacitors. It was observed that the surface area and the quantity and type of phosphorous groups have an important impact on the capacitance. Samples that have higher surface areas and higher amount of phosphate type groups presented higher capacitances.

The results of this work provide a deep insight about the phosphorus functionalization of carbon materials, which has been hardly investigated to date. Moreover, the optimal conditions for preparing phosphorous doped biomass-derived carbons, which have similar electrochemical properties of that of the commercial carbon Supra50, has been defined. The outcomes obtained are of great importance for the future preparation of phosphorus-functionalized carbons to be used as electrode materials in supercapacitor application.

6 Assessment of the work done

6.1 Objectives achieved

The two principal objectives of this work were the preparation and characterization of phosphorous-functionalized carbon materials and the evaluation of their electrochemical performance as electrode materials in supercapacitors. Both objectives were accomplished. In fact, the preparation of the carbon materials not only was successful, as allowed to define the best doping method, but also allowed to determine the relationship between the methods used and the functionalities obtained. Besides, the electrochemical performance of the electrodes was enhanced by the incorporation of phosphorous functionalities.

6.2 Other work carried Out

Other techniques for doping phosphorous were performed. The samples were prepared with double content of phosphoric acid. As only the nitrogen adsorption/desorption isotherms and a few electrochemical measurements were performed due to time limitation, the results obtained are not shown in the present document. However, they will be considered for the future scientific publication that will come out of this work.

6.3 Limitations and future work

One of the principal limitation of this work, was not knowing what to expect from doping carbons with phosphorous. In fact, the initial mixture of phosphoric acid and glucose is still a variable that, in this work, was kept constant due to time limitation. A new approach for future works is to optimize the amount of phosphoric acid introduced on the precursor mixture, as well as optimize the time and temperature used in the hydrothermal process. Such experiments could lead to the incorporation of higher amounts of phosphorous in the form of phosphates, and hence, to achieve higher capacitances.

6.4 Final assessment

The possibility of doing a work in this area, revealed a good adventure. The experience in investigation work plus the knowledge gained in materials science (preparation and characterization) and electrochemical application, gave me a different outlook in the state of energy storing systems.

References

[1] D. S. Su and G. Centi, "A perspective on carbon materials for future energy application," *Journal of Energy Chemistry,* vol. 22, no. 2, pp. 151-173, 2013.

[2] A. González, E. Goikolea, J. A. Barrena, and R. Mysyk, "Review on supercapacitors: Technologies and materials," *Renewable and Sustainable Energy Reviews,* vol. 58, pp. 1189-1206, 2016.

[3] B. E. Conway, *Eletrochemical Supercapacitors*. New York: Kluwer Academic / Plenum Publishers, 1999.

[4] T. K. Enock, C. K. King'ondu, A. Pogrebnoi, and Y. A. C. Jande, "Status of Biomass Derived Carbon Materials for Supercapacitor Application," *International Journal of Electrochemistry,* vol. 2017, pp. 1-14, 2017.

[5] E. G. Calvo, "Síntesis de xerogels de carbono inducida por microondas para su uso como electrodos en supercondensadores," Departamento de Ciencia de los Materiales e Ingeniería Metalúrgica, Universidad de Oviedo, 2013.

[6] A. G. Pandolfo and A. F. Hollenkamp, "Carbon properties and their role in supercapacitors," *Journal of Power Sources,* vol. 157, no. 1, pp. 11-27, 2006.

[7] A. Burke, Z. Lin, and H. Zhao, "Present and Future Applications of

Supercapacitors in Electric and Hybrid Vehicles," *Institute of Trasportation Studies,* 2014.

[8] J. R. Miller and P. Simon, "Eletrochemical Capacitors for Energy Management," *SCIENCE,* vol. 321, pp. 651-652, 2008.

[9] S. Faraji and F. N. Ani, "The development supercapacitor from activated carbon by electroless plating—A review," *Renewable and Sustainable Energy Reviews,* vol. 42, pp. 823-834, 2015.

[10] P. S. A. Burke, "Nanostructured Carbons: Double-Layer Capacitance and More," *Electrochemical Society Interface* vol. 17, pp. 38-43, 2008.

[11] P. Sharma and T. S. Bhatti, "A review on electrochemical double-layer capacitors," *Energy Conversion and Management,* vol. 51, no. 12, pp. 2901-2912, 2010.

[12] M. Endo, T. Takeda, Y. J. Kim, K. Koshiba, and K. Ishii, "High Power Electric Double Layer Capacitor (EDLC's);

from Operating Principle to Pore Size Control

in Advanced Activated Carbons," *Carbon Science,* vol. 1, pp. 117-128, 2001.

[13] X. Chen, R. Paul, and L. Dai, "Carbon-based supercapacitors for efficient energy storage," *National Science Review,* vol. 4, no. 3, pp. 453-489, 2017.

[14] L. L. Zhang and X. S. Zhao, "Carbon-based materials as supercapacitor electrodes," *Chem Soc Rev,* vol. 38, no. 9, pp. 2520-31, Sep 2009.

[15] V. Augustyn, P. Simon, and B. Dunn, "Pseudocapacitive oxide materials for high-rate electrochemical energy storage," *Energy & Environmental Science,* vol. 7, no. 5, 2014.

[16] A. Shaikjee and N. J. Coville, "The synthesis, properties and uses of carbon materials with helical morphology," *Journal of Advanced Research,* vol. 3, no. 3, pp. 195-223, 2012.

[17] F. Ronsse, R. W. Nachenius, and W. Prins, "Carbonization of Biomass," in *Recent Advances in Thermo-Chemical Conversion of Biomass*, 2015, pp. 293-324.

[18] M. Sevilla and R. Mokaya, "Energy storage applications of activated carbons: supercapacitors and hydrogen storage," *Energy Environ. Sci.,* vol. 7, no. 4, pp. 1250-1280, 2014.

[19] Z. Gao, Y. Zhang, N. Song, and X. Li, "Biomass-derived renewable carbon materials for electrochemical energy storage," *Materials Research Letters,* vol. 5, no. 2, pp. 69-88, 2016.

[20] D. Hulicova-Jurcakova, M. Seredych, G. Q. Lu, and T. J. Bandosz, "Combined Effect of Nitrogen- and Oxygen-Containing Functional Groups of Microporous Activated Carbon on its Electrochemical Performance in Supercapacitors," *Advanced Functional Materials,* vol. 19, no. 3, pp. 438-447, 2009.

[21] X.-k. Wan, X.-q. Zou, H.-x. Shi, and D.-h. Wang, "Nitrogen doping of activated carbon loading Fe2O3 and activity in carbon-nitric oxide reaction," *Journal of Zhejiang University-SCIENCE A,* vol. 8, no. 5, pp. 707-711, 2007.

[22] M. Enterría, M. F. R. Pereira, J. I. Martins, and J. L. Figueiredo, "Hydrothermal functionalization of ordered mesoporous carbons: The effect of boron on supercapacitor performance," *Carbon,* vol. 95, pp. 72-83, 2015.

[23] W. Kiciński, M. Szala, and M. Bystrzejewski, "Sulfur-doped porous carbons: Synthesis and applications," *Carbon,* vol. 68, pp. 1-32, 2014.

[24] A. M. Puziy, O. I. Poddubnaya, and A. M. Ziatdinov, "On the chemical structure of phosphorus compounds in phosphoric acid-activated carbon," *Applied Surface Science,* vol. 252, no. 23, pp. 8036-8038, 2006.

[25] J. P. S. Sousa, M. F. R. Pereira, and J. L. Figueiredo, "NO oxidation over nitrogen doped carbon xerogels," *Applied Catalysis B: Environmental,* vol. 125, pp. 398-408, 2012.

[26] J. L. Figueiredo, M. F. R. Pereira, M. M. A. Freitas, and J. J. M. Orfao, "Modification of the surface chemistry of activated carbons," *Carbon* vol. 37, pp. 1379–1389, 1998.

[27] Z. J. Li, B. C. Yang, S. R. Zhang, and C. M. Zhao, "Graphene oxide with improved electrical conductivity for supercapacitor electrodes," *Applied Surface Science,* vol. 258, no. 8, pp. 3726-3731, 2012.

[28] X. Fan, C. Yu, Z. Ling, J. Yang, and J. Qiu, "Hydrothermal synthesis of phosphate-functionalized carbon nanotube-containing carbon composites for supercapacitors with highly stable performance," *ACS Appl Mater Interfaces,* vol. 5, no. 6, pp. 2104-10, Mar 2013.

[29] H. Chen, M. B. Müller, K. J. Gilmore, G. G. Wallace, and D. Li, "Mechanically Strong, Electrically Conductive, and Biocompatible Graphene Paper," *Advanced Materials,* vol. 20, no. 18, pp. 3557-3561, 2008.

[30] S. Talapatra *et al.*, "Direct growth of aligned carbon nanotubes on bulk metals," *Nat Nanotechnol,* vol. 1, no. 2, pp. 112-6, Nov 2006.

[31] C. Gao, Z. Guo, J. H. Liu, and X. J. Huang, "The new age of carbon nanotubes: an updated review of functionalized carbon nanotubes in electrochemical sensors," *Nanoscale,* vol. 4, no. 6, pp. 1948-63, Mar 21 2012.

[32] Y. Wang *et al.*, "Supercapacitor Devices Based on Graphene Materials," *J. Phys. Chem. C* pp. 13103-13107, 2009.

[33] "A Critical Review on Carbon Nanotubes," *International Journal of Constructive Research in Civil Engineering,* vol. 2, no. 5, 2016.

[34] M. Enterría and J. L. Figueiredo, "Nanostructured mesoporous carbons: Tuning texture and surface chemistry," *Carbon,* vol. 108, pp. 79-102, 2016.

[35] M.-M. Titirici, R. J. White, C. Falco, and M. Sevilla, "Black perspectives for a green future: hydrothermal carbons for environment protection and energy storage," *Energy & Environmental Science,* vol. 5, no. 5, 2012.

[36] A. Jain, R. Balasubramanian, and M. P. Srinivasan, "Hydrothermal conversion of biomass waste to activated carbon with high porosity: A review," *Chemical Engineering Journal,* vol. 283, pp. 789-805, 2016.

[37] M. Sevilla and A. B. Fuertes, "Chemical and structural properties of carbonaceous products obtained by hydrothermal carbonization of saccharides," *Chemistry,* vol. 15, no. 16, pp. 4195-203, 2009.

[38] C. Falco *et al.*, "Tailoring the porosity of chemically activated hydrothermal carbons: Influence of the precursor and hydrothermal carbonization temperature," *Carbon,* vol. 62, pp. 346-355, 2013.

[39] A. Stein, Z. Wang, and M. A. Fierke, "Functionalization of Porous Carbon Materials with Designed Pore Architecture," *Advanced Materials,* vol. 21, no. 3, pp. 265-293, 2009.

[40] J. B. Parra, J. C. d. Susa, R. C. Bansal, J. J. Pis, and J. A. Pajares, "Characterizartion of Activated Carbons by the BET Equation - An Alternative Apporach," pp. 51-66, 1994.

[41] L. Verhoeven and P. Lodewyckx, "Comparison of Duvinin-Rradushkevich micropore volumes obtained from N2, CO2 and H2O-adsorption isotherms."

[42] P. v. d. Heide, *X-ray Photoelectron Spectroscopy: An Introduction to Principles and Pratices*. 2012.

[43] C. Sangwichien, G. L. Aranovich, and M. D. Donohue, "Density functional theory predictions of adsorption isotherms with hysteresis loops," *Elsevier Science,* vol. Colloids and Surfaces, pp. 313-320, 2002.

[44] A. M. Puziy, O. I. Poddubnaya, R. P. Socha, J. Gurgul, and M. Wisniewski, "XPS and NMR studies of phosphoric acid activated carbons," *Carbon,* vol. 46, no. 15, pp. 2113-2123, 2008.

[45] A. M. K. Morawa Eblagon,

M.F.R. Pereira,

J.L. Figueiredo, "Cutting the green waste. Structure - performance relationship in fuctionalised carbon xerogels for hydrolysis of cellobiose," *Wiley-VCH.*

Appendix A – SEM images

SEM images at 2 and 20 µm for the two methods employed of the prepared the materials.

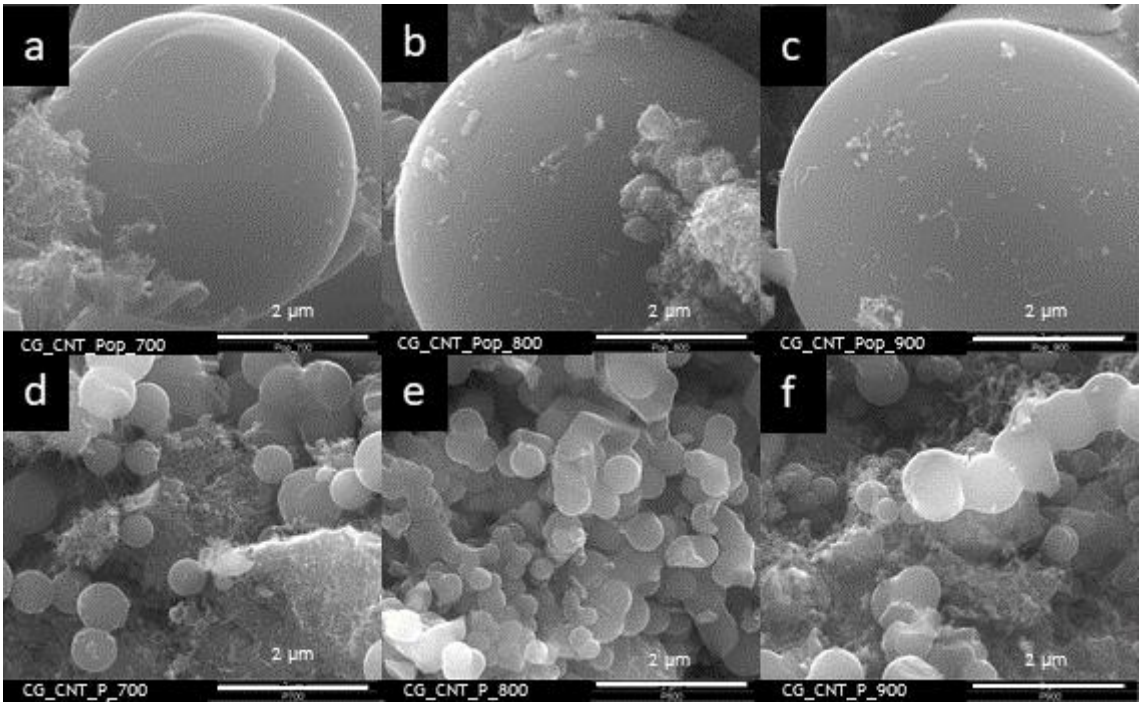

Figure 31 - SEM images at 2 µm for: a – CG_CNT_Pop_700, b - CG_CNT_Pop_800, c - CG_CNT_Pop_900, d - CG_CNT_P_700, CG_CNT_P_800 and CG_CNT_P_900.

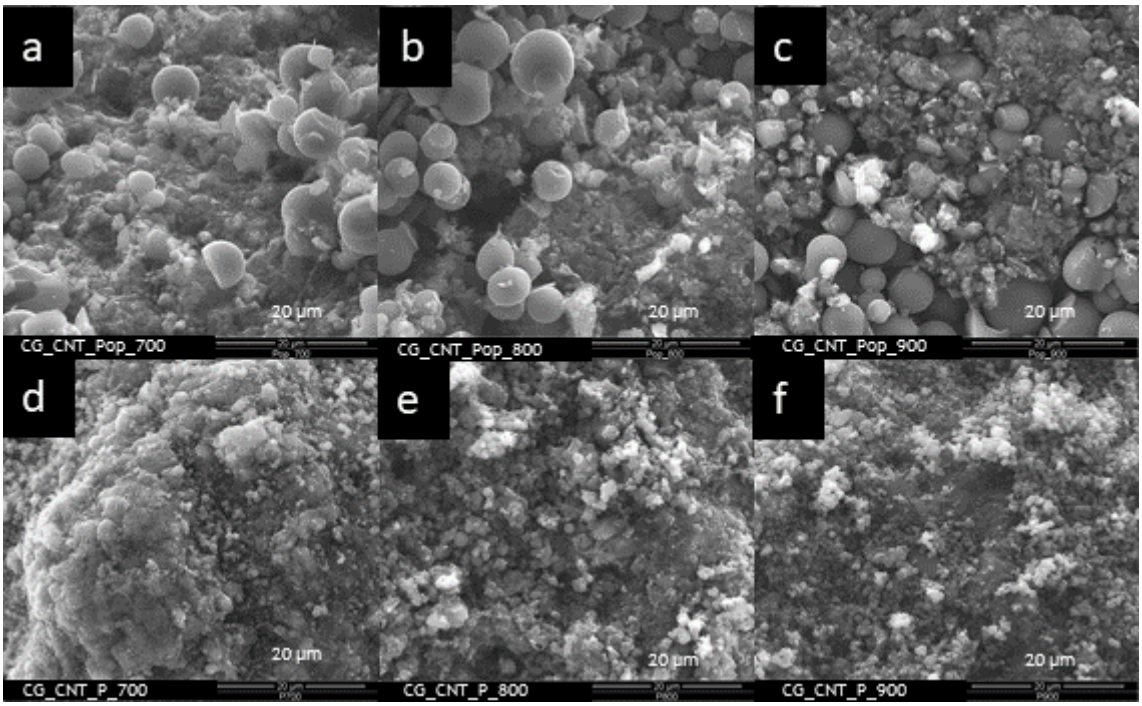

Figure 32 - SEM images at 20 µm for: a – CG_CNT_Pop_700, b - CG_CNT_Pop_800, c - CG_CNT_Pop_900, d - CG_CNT_P_700, CG_CNT_P_800 and CG_CNT_P_900.

Appendix B - Cyclic voltammetry in three-electrode

Example of CVs performed at a scan rate of 2, 10, 20 and 50 mV s^{-1} and a constant voltage window of 0.8 V for samples CG_CNT_Pop_800 (Figure 34) and CG_CNT_P_800 (Figure 35).

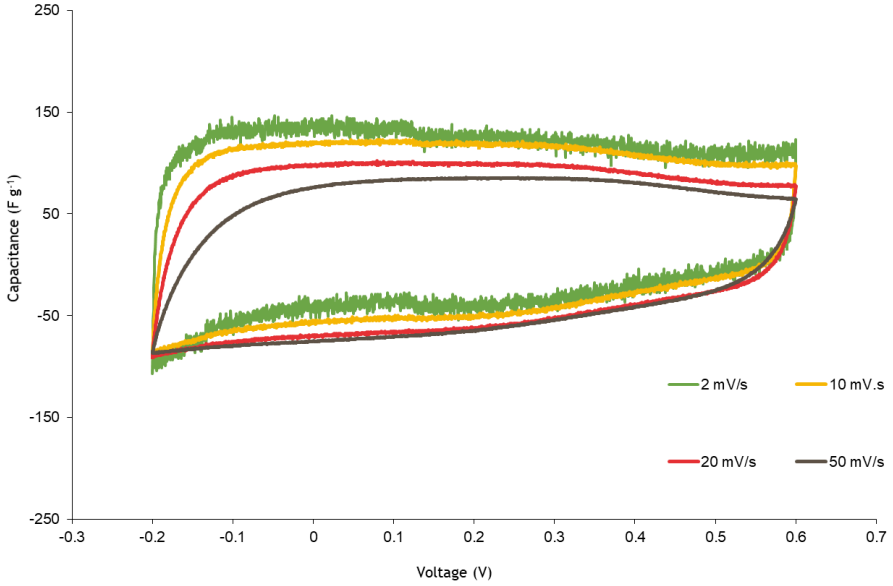

Figure 33 -Cyclic voltammetries for sample CG_CNT_Pop_800 at a voltage window of 0.8 and different scan rates

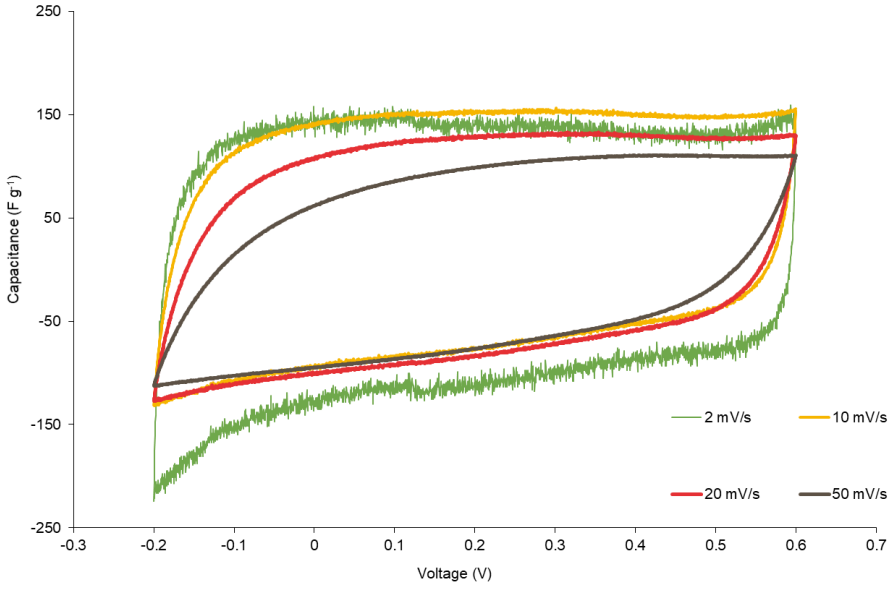

Figure 34 - Cyclic voltammetries for sample CG_CNT_P_800 at a voltage window of 0.8 V and different scan rates

Appendix C – Cyclic voltammetry in two-electrode

Example of cyclic voltammetries performed in a voltage window of 0.6, 0.8, 1 and 1.2 V at a constant scan rate of 2 mV s^{-1} for sample CG_CNT_Pop_800 (Figure 36) and sample CG_CNT_P_800 (Figure 37).

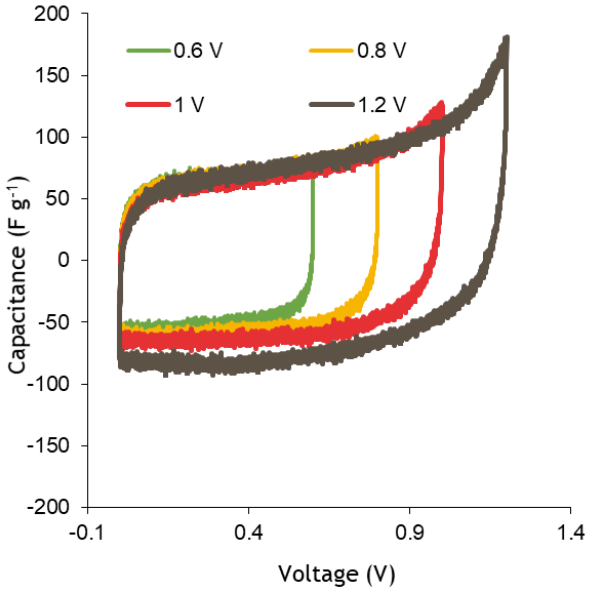

Figure 35 – Cyclic voltammetries of sample CG_CNT_Pop_800 at different voltage windows and a constant scan rate of 2 mV s^{-1}

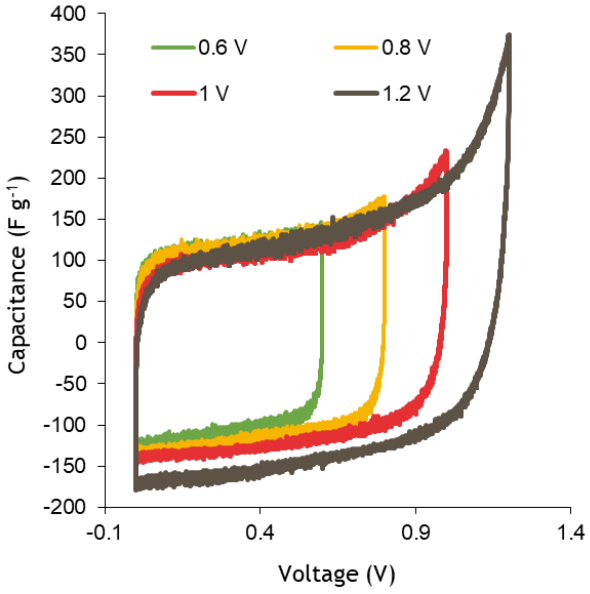

Figure 36 - Cyclic voltammetries of sample of CG_CNT_P_800 at different voltage windows and a constant scan rate of 2 mV s^{-1}

Appendix D - Calculation of capacitance throw galvanostatic charge/discharge method

The capacitance obtained by the galvanostatic charge/discharge curve is calculated by using equation 3.

$$C = \frac{2I \times (t2 - t1)}{v1 - v2} \quad (4)$$

Where, I is the current density applied, v1 and v2 are the maximum and final potential values, respectively and t1 and t2 are time values corresponding to the maximum and final potential values, respectively. A detailed scheme is showed in Figure 38.

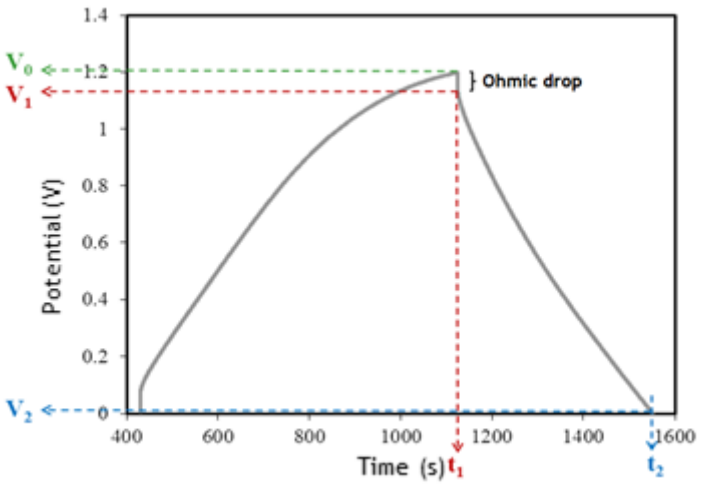

Figure 37 - Example of a galvanostatic charge/discharge curve